BAOJ Chemistry

Alfons Penzkofer, et al., BAOJ Chem 2016, 2: 2
2: 008

Research article

Photodynamics of Photo-Activated BLUF Coupled Endonuclease III Mutant RmPAE from Mesophilic, Pigmented Bacterium *Rubellimicrobium mesophilum* Strain MSL-20^T

Alfons Penzkofer[1*], Yama Atri[2], Komal Sharma[2], Sindhu K Veetil[2] and Suneel Kateriya[2,3]

[1] *Institut für Experimentelle und Angewandte Physik, Universität Regensburg, Universitätsstraße 31 D-93053 Regensburg, Germany*

[2] Department of Biochemistry, University of Delhi South Campus, New Delhi, India-110021

[3] School of Biotechnology, Jawaharlal Nehru University, New Delhi, India-110067

Abstract

The pink to light reddish-pigmented bacterium *Rubellimicrobium mesophilum* strain MSL-20^T contains a BLUF coupled endonuclease III of unknown function. A purified recombinant triple mutated sample of the BLUF coupled endonuclease III (F5Y, N27H, A87W) named RmPAE (*Rubellimicrobium mesophilum* Photo-Activated Endonuclease) was produced and characterized by optical spectroscopic methods. The BLUF domain photo-cycling dynamics occurred with high efficient blue-light induced signaling state formation (quantum yield of signaling state formation $\phi_s \approx 0.6$), small spectral red-shift ($\delta\lambda_{s,r} \approx 5.4$ nm), and slow thermal activated dark recovery to the receptor state ($\tau_{rec} \approx 20$ min at room temperature). An apparent RmPAE melting temperature of $\vartheta_m \approx 63$ °C was determined by stepwise sample heating and absorption spectrum analysis. The photo-degradation of RmPAE in the signaling state was determined by prolonged intense blue-light exposure. An irreversible flavin photo-degradation occurred with quantum yield of $\phi_D \approx 2.6\times10^{-5}$. Schemes of the photo-cycling and the photo-degradation dynamics are presented. Engineered RmPAE may find application as light guided DNA cutter in optogenetic applications.

Introduction

The pink to light reddish-pigmented alpha proteobacterium *Rubellimicrobium mesophilum* strain MSL-20^T (= DMS 19309^T = KCTC 22012^T) was isolated from a soil sample of Bigeum island in Korea [1]. *R. mesophilum* strain MSL-20^T cells are Gram-negative, motile, non-flagellated, irregular rods (size 0.4-0.7 × 1.6-3.4 μm^2) as characterized in [1]. *R. mesophilum* belongs to the abundant marine *Roseobacter* lineage [2]. The genome sequence of *R. mesophilum* strain MSL-20^T is reported in [3]. It consists of 4,927,676 base pairs. The total number of genes is 5138, of which 2915 are protein-coding genes. One of these genes is coding for BLUF coupled restriction Endonuclease III (BLUF-EndoIII). It was identified through metagenome analysis using a BLUF domain containing protein as a template using Conserved Domain Search tool in NCBI portal [4]. The schematic BLUF and Endonuclease III structure is shown in Fig.1a, and the primary amino acid sequence of BLUF-EndoIII is shown in Fig.1b.

The BLUF-EndoIII protein was analyzed for flavin chromophore binding residues. A sequence alignment was carried out between the BLUF domain of BLUF-EndoIII and the BLUF domain of AppA from *Rhodobacter sphaeroides* [5] using BioEdit software [6]. The result is shown in Fig.1c. The conserved residues are highlighted by white letters in grey background and similar residues are highlighted by black letters in grey background. The vertical arrows indicate flavin binding amino acids. At the flavin binding positions 5, 27 and 87 the amino acids of AppA and BLUF-EndoIII are different. Especially at position 7 AppA has a Tyr residue while BLUF-EndoIII has a Phe residue and there is missing any Tyr residue in BLUF-EndoIII. Tyr residues adjacent to flavin are essential for the typical photo-cycling action of BLUF domains (for reviews see [7-9]) and the photo-activation of BLUF domain coupled cyclases (PAC proteins) (see [10] and references therein). Therefore here the BLUF domain of BLUF-EndoIII was triple mutated to BLUF-EndoIII F5Y, N27H, A87W. This engineered mutated protein is a putative photo-activated endonuclease (PAE protein) and is named RmPAE (photo-activated endonuclease from *R. mesophilum*).

In this paper the expression of RmPAE is described and the photo-physical dynamics is studied in detail. Different to other BLUF and PAC proteins RmPAE exhibits smaller signaling state spectral red-shift, slower signaling state recovery to the receptor state, and in the signaling state part of the BLUF domain active flavin (likely the FAD fraction) is released to BLUF domain inactive

***Corresponding author:** Alfons Penzkofer, Institut für Experimentelle und Angewandte Physik, Universität Regensburg, Universitätsstraße 31, D-93053 Regensburg, Germany, E-mail:alfons.penzkofer@physik.uni-regensburg.de

Sub Date: December 29, 2015, **Acc Date:** January 20, 2016, **Pub Date:** January 25, 2016.

Citation: Alfons Penzkofer, Yama Atri, Komal Sharma, Sindhu K Veetil, Suneel Kateriya (2016) Photodynamics of Photo-Activated BLUF Coupled Endonuclease III Mutant RmPAE from Mesophilic, Pigmented Bacterium *Rubellimicrobium mesophilum* Strain MSL-20^T. BAOJ Chem 2: 008.

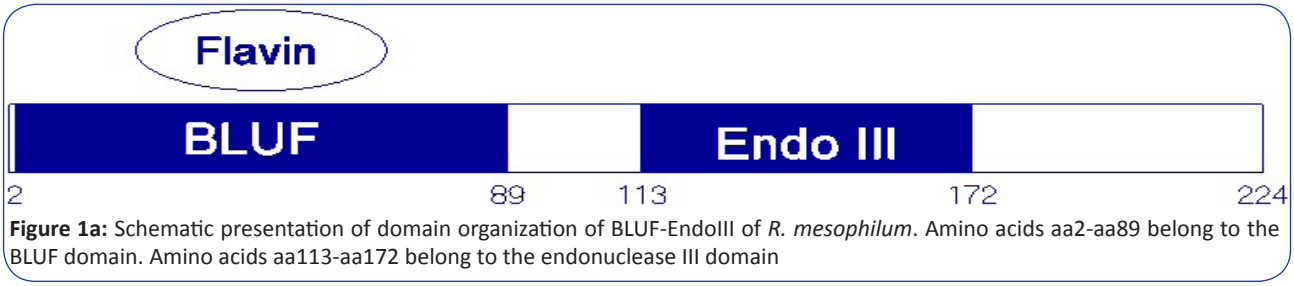

Figure 1a: Schematic presentation of domain organization of BLUF-EndoIII of *R. mesophilum*. Amino acids aa2-aa89 belong to the BLUF domain. Amino acids aa113-aa172 belong to the endonuclease III domain

MRLVFSSVRT DSEPATVGGI LQVSRRNNPR DGVTGALLSS RTRFVQLLEG DAAGLDRCFA 60

RIQRDARHRD IRVLLSGPTR ELLFPEAPML GIEAAGLDSP VAAALSDDAP PDRVMEILRA 120

LARRTDPQPA EVPEADASLV ALRRIHRAAR HILDDHLSRS EMPPDTLERL AASLTRQAAQ 180

AGDLHRRLSA ASSADPDHRT EAQRFHELLQ AAQREVGRRL GRLD 224

Figure1b: Amino acid sequence of the natural BLUF-EndoIII protein of *R. mesophilum*.

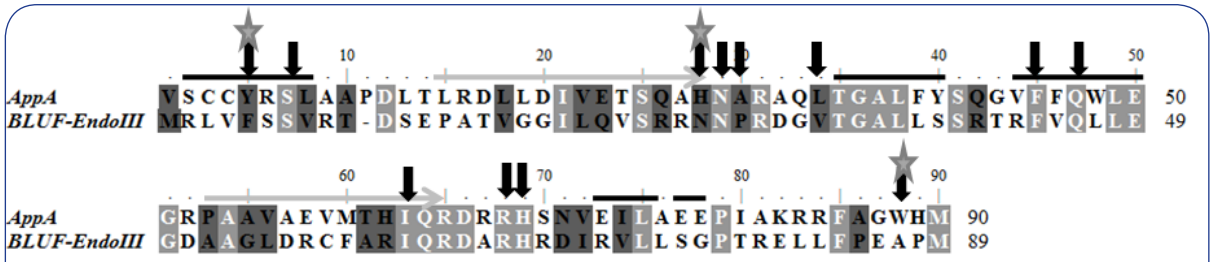

Figure 1c: Sequence alignment of BLUF domain of BLUF-EndoIII with BLUF domain AppA from *Rhodobacter sphaeroides* [5]. See main text. Stars represent positions of mutated amino acids for RmPAE (F5Y, N27H, A87W). Grey horizontal arrows represent α-helices, and black horizontal bars indicate β-sheets.

(improper bound or domain released) flavin. The receptor-state signaling-state photo-cycling dynamics is presented in a refined photo-cycle scheme and a ground-state and excited-state reaction coordinate scheme. Energetic and kinetic parameters are extracted. Preliminary functional characterization of the RmPAE gene paves way to develop a novel optogenetic tool.

Experimental

Protein Sample Preparation and Biochemical Characterization

Bioinformatic analysis of BLUF-Endonuclease III: The gene coding for BLUF coupled Endonuclease III from *R. mesophilum*, BLUF-EndoIII, was identified through metagenome analysis using a BLUF domain containing protein as template. Domain analysis of the putative BLUF-EndoIII was done using Conserved Domain (CD) Search tool at NCBI portal (http://www.ncbi.nlm.nih.gov/Structure/cdd/wrpsb.cgi) [4]. The protein BLUF-EndoIII was analyzed for flavin chromophore binding residues. Sequence alignment was carried out between BLUF domains of BLUF-EndoIII and AppA from *Rhodobacter sphaeroides* [5], (PDB Id: 1YRX) using BioEdit software [6].

Generation and cloning of mutated BLUF-Endonuclease III (RmPAE): Codon optimized gene of BLUF-EndoIII was synthesized for expression in *Escherichia coli* from BIOLINKK, New Delhi, India. Three residues were mutated in the synthesized gene (F5Y, N27H and A87W). These mutations were based on sequence analysis with AppA protein from *Rhodobacter sphaeroides*, (PDB Id: 1YRX) in order to obtain a photo-biologically active BLUF domain. The gene was cloned into pASKIBA43PLUS vector (IBA, Göttingen, Germany) between BamH1 and Xho1 restriction sites.

Heterologous expression and purification of RmPAE in *E .coli*: Hexa-histidine tagged mutated BLUF-EndoIII pASK construct was transformed into BL21 (λDE3) cells and grown in terrific broth medium (TBM) at 37 °C till the optical density at 600 nm reached 0.8. The cells were induced with 0.02 mg/ml anhydrotetracycline (Cat. No. 2-0401-002, Nova Biological Systems Pvt. Ltd, Novabiosys, India) for 4 h at 16 °C in dark. The recombinant protein was purified from the soluble fraction with Co^{++} IMAC resin (Clontech, Takara Bio Company, India) according to the manufacturer's instructions. The purified protein was dialyzed against pH 7.5 phosphate buffer consisting of 10 mM Na_2HPO_4/ NaH_2PO_4 and 10 mM NaCl. SDS-PAGE and immunoblotting of

the purified protein elutions obtained were performed using Penta His-tag specific antibody (Qiagen, Hilden, Germany) at 1:5000 dilution in 1X PBS (phosphate buffer saline) and horseradish peroxidase (HRP) conjugated goat anti- mouse antibody (1:5000 dilution) using enhanced chemiluminescence (ECL) method.

Endonuclease assay of purified mutated BLUF-EndoIII (RmPAE): For performing endonuclease assay, pASK construct was incubated with purified mutated BLUF-EndoIII enzyme and exposed to blue light. The pASK construct alone was taken as control.

Optical Spectroscopic Investigations

The RmPAE protein in pH 7.5 phosphate buffer (10 mM Na_2HPO_4/NaH_2PO_4, 10 mM NaCl, 25 % glycerol) was stored at -80 °C. Before usage it was thawed and then stored in the dark at 4 °C. The measurements were carried out at room temperature except stated differently. The RmPAE solutions were investigated in fused silica ultra micro cells (inner size 1.5×3×5 mm^3).

Transmission measurements, $T(\lambda)$, were carried out with a spectrophotometer (Cary 50 from Varian). Attenuation coefficient spectra were calculated by the relation $\alpha(\lambda)=-\ln[T(\lambda)]/\ell$, where ℓ is the sample length. The attenuation coefficient α is composed of absorption, α_{abs}, and scattering, α_{sca}, contributions according to $\alpha(\lambda) = \alpha_{abs}(\lambda) + \alpha_{sca}(\lambda)$.

Fluorescence spectroscopic measurements were carried out with a spectrofluorimeter (Cary Eclipse from Varian). Fluorescence quantum distributions $E_F(\lambda)$ were determined from fluorescence emission spectrum measurements at fixed excitation wavelengths $\lambda_{F,exc}$ [11,12]. The dye rhodamine 6G in methanol was used as reference standard for calibration ($\phi_{F,ref}$ = 0.94 [13]). The fluorescence quantum yield ϕ_F is determined by the relation $\phi_F=\int_{em} E_F(\lambda)\, d\lambda$ where the integration runs over the emission wavelength region.

For absorption spectroscopic photo-cycling investigations, RmPAE samples were brought to the signaling state (light-adapted state) by exposure with a light emitting diode (LED 455 nm from Thorlabs). The sample solution in a 1.5×3×5 mm^3 cell in the Cary 50 spectrophotometer for transmission measurement was irradiated with the LED transverse to the transmission detection path (exposed area 3×5 mm^2, sample thickness along excitation path 1.5 mm, sample thickness along transmission detection path 3 mm). The excitation power P_{exc} was measured with a power meter (model PD 300-UV-SH photodiode detector head with NOVA power monitor from Ophir), and the excitation intensity I_{exc} was calculated($I_{exc} = P_{exc} / A_{cell}$, A_{cell} = 0.15 cm^2).

The fluorescence spectrum recovery after signaling state formation was studied by transferring the RmPAE sample after photo-excitation in the Cary 50 spectrophotometer to the Cary eclipse fluorimeter and measuring fluorescence emission spectra at certain times after excitation light switch-off.

Fluorescence lifetime measurements were performed using second harmonic light pulses of a mode-locked titanium sapphire laser (Hurricane from Spectra-Physics, wavelength 400 nm) for sample excitation. The fluorescence signal was detected with either a micro-channel-plate photomultiplier (Hamamatsu type R1564U-01, used laser pulse duration ≈ 3 ps, time-resolution ≈ 500 ps) or an ultrafast streak camera (type C1587 temporal disperser with M952 high-speed streak unit from Hamamatsu, used laser pulse duration ≈ 1 ps, time resolution ≈ 10 ps).

The thermal stability of the protein was investigated by stepwise sample heating up and then cooling down whereby transmission spectra were measured. The apparent protein melting temperature of RmPAE was determined by analysis of the occurring absorption spectral changes [14]. Heating up to 85.2 °C caused complete irreversible protein denaturation with flavin cofactor release. The flavin cofactor composition (FAD, FMN and/or riboflavin) was estimated from fluorescence quantum yield measurements after the sample heating-cooling cycle [10].

The photo-degradation of RmPAE in the signaling state was studied by sample exposure with our light emitting diode (LED 455 nm from Thorlabs) as in the case of the photo-cycling studies but with higher excitation intensity and longer exposure time.

Results

Biochemical Characterization

The BLUF coupled Endonuclease III from *R. mesophilum* was analyzed for studying domain organization of the protein. Upon conserved domain analysis, light sensitive BLUF domain was found at the N-terminus spanning from 2-89 amino acids, which was coupled to the C-terminus endonuclease domain located between 113-172 amino acids (see Fig.1a). The Endonuclease III from *R. mesophilum* was found to belong to the Endonuclease III super-family which includes endonuclease III (DNA-(apurinic or apyrimidinic site) lyase), alkylbase DNA glycosidases (Alka-family) and other DNA glycosidases.

Multiple sequence alignment was performed between the BLUF domains from BLUF-EndoIII and AppA protein from *Rhodobacter sphaeroides*. This was done to analyze the conservation of key amino acids involved in flavin binding with respect to a canonical BLUF protein in order to ascertain a potentially active photoreceptor. The residues that line the flavin binding pocket in the BLUF-EndoIII are F5, S7, N27, N28, P29, L37, F44, Q46, I62, R67, H68 and A87, (see Fig.1c). On comparison with AppA protein from *R. sphaeroides*, three residues of BLUF-EndoIII namely, F5, N27 and A87 were found to be different to their corresponding residues in AppA protein. The codon optimized gene synthesized for BLUF-EndoIII had F5Y, N27H and A87W mutations (this triple mutated BLUF-EndoIII is called RmPAE).

The triple mutated BLUF-EndoIII gene was cloned between BamH1 and Xho1 into the pASK vector (see top part of Fig.2a). The 6x His-tagged BLUF-EndoIII was heterologously expressed in *E. coli* upon anhydrotetracycline induction and the purified soluble protein was detected as a ~25 kDa band upon immunoblotting, (see bottom

part of Fig.2a). The protein was dialyzed against pH 7.5 phosphate buffer consisting of 10 mM Na_2HPO_4/NaH_2PO_4 and 10 mM NaCl.

The enzymatic activity of the triple mutated BLUF-EndoIII was examined. Since BLUF-EndoIII is an endonuclease belonging to a superfamily that includes DNA lyase, alkylbase DNA glycosidases and other DNA glycosidases, we checked for the enzyme activity by looking for DNA cleavage products visible on gel. The purified photoreceptor coupled enzyme was added to DNA construct with and without appropriate buffer (e.g. FastDigest™ buffer) in the presence of blue light and the reaction products were analyzed on DNA gel. pASK DNA construct was digested by the enzyme during incubation time (first and second row of Fig.2b) as is seen by comparison with the gel trace of the pASK DNA construct alone (third row of Fig.2b). Triple mutated BLUF-EndoIII was found to be digesting/degrading the pASK vector.

Future perspectives of this novel BLUF coupled endonuclease include the determination of the mechanism of its light-gated activity.

Spectroscopic characterization of unexposed RmPAE

Absorption behavior: The attenuation coefficient spectrum α(λ) of a fresh thawed dark-adapted RmPAE sample is displayed by the solid curve in the top part of Fig.3. It was obtained by sample centrifugation with 4400 rpm for 15 min in an Eppendorf centrifuge 5702R at 4 °C. The dotted curve in the top part of Fig.3 shows the approximate scattering contribution $\alpha_{sca}(\lambda)$. It was determined by an empirical power law fit [15] of $\alpha_{sca}(\lambda) = \alpha_{sca}(\lambda_0)\,(\lambda_0/\lambda)^{\gamma}$ with λ_0 = 800 nm, $\alpha_{sca}(\lambda_0)$ = 0.0065 cm^{-1}, and γ = 4 (γ ≤ 4 depends on

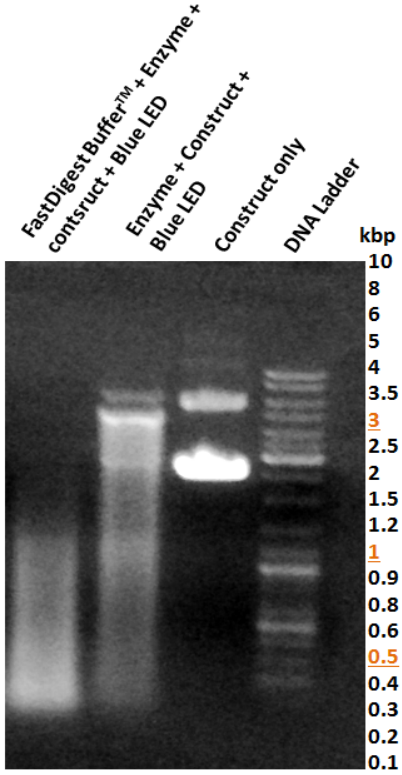

Figure 2b: Endonuclease assay of purified RmPAE. First column: pASK construct was incubated with purified mutated BLUF-Endonuclease III enzyme in FastDigest™ buffer for 30 min under blue light .Second column: pASK vector construct was incubated with purified BLUF-EndonucleaseIII enzyme without buffer for 30 min under blue light. Third column: pASK construct only. Forth column: DNA ladder.

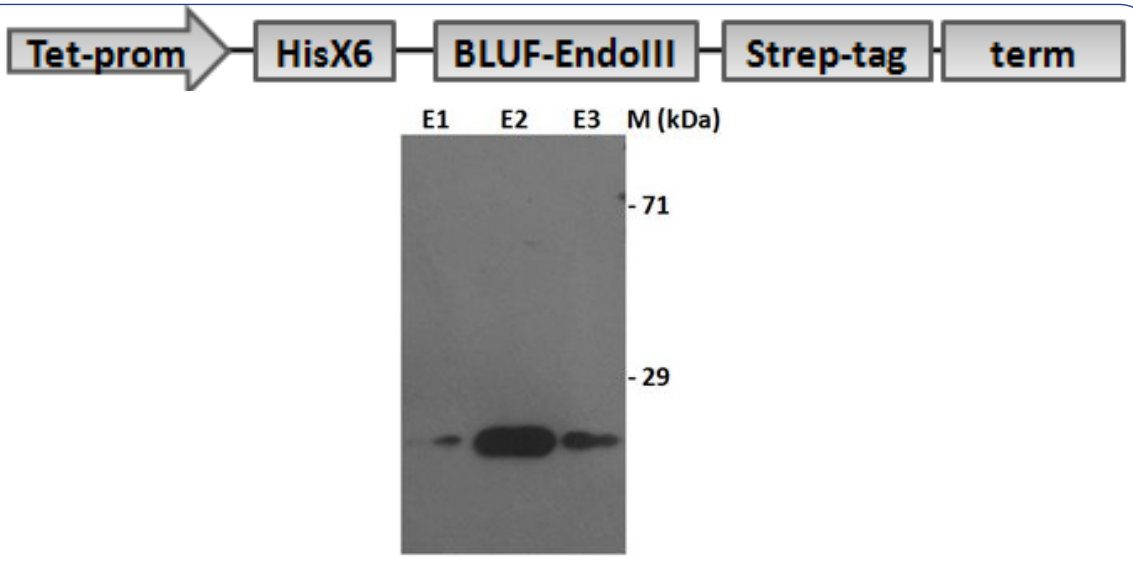

Figure 2a: Heterologous expression of triple mutated BLUF-EndoIII RmPAE. Top part: Schematic diagram of pASK-BLUF-EndoIII construct. The tetracycline promoter was upstream of Hexa-histidine tag located at the 5' terminus of BLUF-EndoIII gene cloned between BamH1 and Xho1 followed by another tag of Streptavidin at the 3' terminus ending with the terminator sequence.

Bottom part: Immunoblot of RmPAE elution fractions obtained after affinity purification as probed by His-specific antibody. E1, E2 and E3: Elution fractions 1, 2 and 3.

the scattering particle size with smaller γ for larger particle size). The dashed curve shows the approximate absorption coefficient spectrum contribution $\alpha_{abs}(\lambda) = \alpha(\lambda) - \alpha_{sca}(\lambda)$. For comparison the dash-dotted curve shows the absorption coefficient spectrum of FMN in aqueous solution at pH 7 normalized to the same absorption coefficient as the RmPAE sample at λ = 460 nm. For λ > 310 nm the absorption spectrum of RmPAE is determined by the flavin cofactor absorption. Below 310 nm the RmPAE apoprotein absorption contributes to the absorption mainly due to Tyr, Trp and Phe absorption (1 RmPAE protein molecule contains 1 Tyr, 1 Trp and 4 Phe residues). The absorption cross-section spectra $\sigma_{abs}(\lambda)$ of FMN in aqueous solution at pH 7 (solid curve, from [16]), FAD in aqueous solution at pH 7 (dashed curve, from [17]), Trp (dotted curve, from [18]), Tyr (dash-dotted curve, from [18]), and Phe (dashed triple-dotted curve, from [18]) are displayed in the bottom part of Fig.3.

The flavin S_0-S_1 absorption band of RmPAE exhibits vibronic structure indicating an ordered arrangement of flavin in the BLUF domain. The long-wavelength absorption tail of flavin in RmPAE is steep. On the contrary the absorption spectrum of FMN in neutral aqueous solution is smeared out with a less steeply rising long-wavelength absorption tail due to inhomogeneous broadening in the unstructured water solution.

The flavin number density $N_{Fl,0}$ of the centrifuged sample was determined by equating the S_0-S_1 absorption cross-section integral of the flavin in RmPAE, $\int_{S_0-S_1}\sigma_{abs,Fl}(\tilde{\nu})d\tilde{\nu}$, to the S_0-S_1 absorption cross-section integral of FMN (flavin mononucleotide) in aqueous solution at pH 7 (from [16]), $\int_{S_0-S_1}\sigma_{abs,FMN}(\tilde{\nu})d\tilde{\nu}$, where $\tilde{\nu}=\lambda^{-1}$ is the wavenumber. This equal setting gives flavin number density

$$N_{Fl,0}=\int_{S_0-S_1}\alpha_{abs,Fl}(\tilde{\nu})d\tilde{\nu}\Big/\int_{S_0-S_1}\sigma_{abs,FMN}(\tilde{\nu})d\tilde{\nu}$$

. Using S_0-S_1 upper wavelength borders of $\lambda_{u,RmPAE}$ = 396 nm and $\lambda_{u,FMN}$ = 399 nm we get $\int_{S_0-S_1}\alpha_{abs,Fl}(\tilde{\nu})d\tilde{\nu}$ = 8192.85 cm^{-2} and $\int_{S_0-S_1}\sigma_{abs,FMN}(\tilde{\nu})d\tilde{\nu}$ = 1.71×10^{-13} cm giving $N_{Fl,0}$ = 4.79×10^{16} cm^{-3} (concentration $C_{Fl,0}$ = 7.96×10^{-5} mol dm^{-3}).

The number density $N_{RmPAE\ apoprotein}$ of RmPAE apoprotein may be determined by using the relation

$$N_{RmPAE\ apoprotein}\approx\left|\alpha_{abs,RmPAE}(270nm)-N_{Fl,0}\sigma_{Fl}(270nm)\right|\Big/\left|n_{Tyr}\sigma_{Tyr}(270nm)+n_{Trp}\sigma_{Trp}(270nm)\right|$$

. Insertion of values ($\alpha_{abs,RmPAE}$ (270 nm) = 10.91 cm^{-1}, σ_{Fl}(270 nm) ≈ σ_{FMN}(270 nm) = 1.33×10^{-16} cm^{-2} [16], n_{Tyr} = 1, σ_{Tyr}(270 nm) = 4.67×10^{-18} cm^2 [18], n_{Trp} = 1, and σ_{Trp}(270 nm) = 1.99×10^{-17} cm^2 [18]) gives $N_{RmPAE\ apoprotein}$ ≈ 1.85×10^{17} cm^{-3}.

The flavin loading factor of RmPAE, $\kappa_{Fl,load}$, is obtained from $N_{Fl,0}$ and $N_{RmPAE\ apoprotein}$ to be $\kappa_{Fl,load} = N_{Fl,0}/N_{RmPAE\ apoprotein}$ ≈ 0.26. On the average roughly each fourth RmPAE apoprotein non-covalently binds a flavin cofactor molecule. The RmPAE proteins form nano-clusters as is indicated by the RmPAE scattering coefficient spectrum $\alpha_{sca}(\lambda)$ (dotted curve in top part of Fig.3). An estimate of the average cluster size is given in section S1 of the Supplementary material (average number of RmPAE proteins in a nano-cluster is calculated to be β_m = 106).

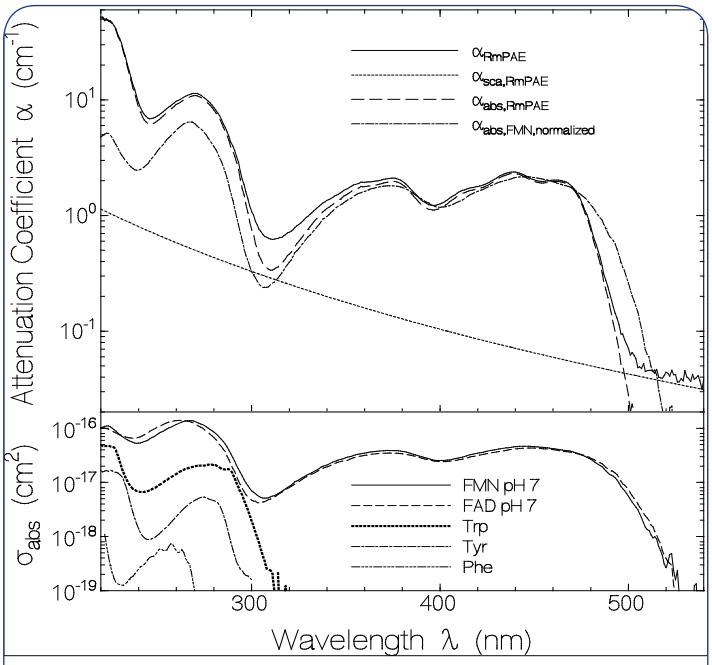

Figure 3: Top part: Attenuation coefficient behavior of a sample of RmPAE in pH 7.5 phosphate buffer.

Bottom part: absorption cross-section spectra of FMN in aqueous solution at pH 7, FAD in aqueous solution at pH 7, Trp, Tyr, and Phe.

Fluorescence behavior: Fluorescence quantum distributions $E_F(\lambda)$ of a fresh unexposed RmPAE sample (only used above in Fig.3 for absorption spectra measurements) are shown by solid curves in Fig.4 for fluorescence excitation wavelengths $\lambda_{F,exc}$ = 450 nm (top part), 350 nm (middle part), and 270 nm (bottom part). The corresponding fluorescence quantum yields $\phi_F=\int E_F(\lambda)d\lambda$ are listed in the legends of the subfigures. It should be noticed that the sample exposure for fluorescence signal measurement causes some BLUF domain signaling state formation and accompanied proper non-covalently bound flavin release to improper positioned flavin of increased fluorescence efficiency within the signaling-state lifetime (see below).

For $\lambda_{F,exc}$ = 450 nm the fluorescence results from emission of excited non-covalently bound fully oxidized neutral flavin in the BLUF domain (peak position around 495 nm) and free fully oxidized neutral flavin (peak position around 530 nm, for different redox states and ionization states of flavins see [19]). The obtained fluorescence quantum yield is ϕ_F(450 nm) = 0.0065±0.0005. The fluorescence quantum yield of non-covalently bound flavin cofactor is strongly quenched by BLUF-type reductive electron transfer from Tyr to photo-excited flavin (see [10] and references therein).

For $\lambda_{F,exc}$ = 350 nm again non-covalently bound flavin and free flavin emission is observed for λ > 480 nm. Additionally a short wavelength tail extending down to 370 nm is present. It may be

due to nano-cluster color-center emission [20,21], to lumichrome contribution [22], and to contribution of quinoxaline hydrolysis products of flavin [23] (likely QO1 and QO4 of [23]). The combined fluorescence quantum yield is $\phi_F(350\ nm) = 0.00879 \pm 0.0005$.

For $\lambda_{F,exc} = 270$ nm Tyr (shoulder at 308 nm), Trp (peak at 335 nm) and flavin (peak around 524 nm) contribute to the fluorescence emission. The combined fluorescence quantum yield is $\phi_F(270\ nm) = 0.0192 \pm 0.001$. The Tyr emission is strongly quenched (Tyr shoulder small compared to Trp peak) due to efficient Förster-type [11] Tyr to Trp energy transfer (see supporting information to [24]). The Trp emission is thought to be quenched by efficient Förster-type energy transfer to flavin (fluorescence quantum yield of Trp in aqueous solution is $\phi_F = 0.13$ [25]).

The dependence of the fluorescence quantum distribution of the investigated unexposed RmPAE sample on the fluorescence excitation wavelength is presented in detail in Fig.S1 of the Supplementary material. There spectra are shown for fluorescence excitation wavelengths in the range from 470 nm to 230 nm in steps of 10 nm. The dependence of the corresponding fluorescence quantum yield on the fluorescence excitation wavelength is shown in Fig.S2 by the solid line connected circles. For $\lambda_{F,exc} \geq 470$ nm the fluorescence efficiency increased because of dominant absorption of free flavin. The presence of lumichrome, quinoxaline hydrolysis products (QO1, QO2, QO3, QO4 of [23]) and possible nano-cluster color center increases the fluorescence efficiency between 410 nm and 320 nm. For $\lambda_{F,exc} \leq 310$ nm the fluorescence is dominated by Trp emission. The highest fluorescence quantum yield is observed for $\lambda_{F,exc} = 300$ nm and 290 nm where the absorption is dominated by Trp which has the strongest fluorescence efficiency.

A temporal fluorescence trace (average of 10 measured traces) of a dark-adapted centrifuged RmPAE sample measured at ϑ = 21.3 °C with our microchannel-plate photomultiplier tube is displayed in the top part of Fig.5a (thick solid curve, maximum signal height is normalized to 1, i.e. $S_{F,da}(t)/S_{F,da,max}$ is presented) together with the system response function (dotted line, Rayleigh scattered light at excitation wavelength from a cell filled with water was registered). This sample was previously only exposed for an absorption spectrum measurement (negligible excitation intensity [24]) and three fluorescence spectra measurements ($\lambda_{F,exc}$ = 450 nm, 350 nm and 270 nm, non-negligible excitation intensity for partial signaling state formation [24]). The fluorescence trace exhibits the presence of a free flavin contribution shown by the dashed curve (convoluted single-exponential trace of amplitude fraction $a_{free} = 0.124$ and fluorescence lifetime $\tau_{F,free} = 5$ ns, see section S3 of Supplementary material for the applied convolution analysis). The solid curve in the bottom part of Fig.5a shows the fluorescence contribution of the non-covalently bound flavin $S_{F,b,da}(t)/S_{F,b,da,max}$. This fluorescence trace fits well to a convoluted bi-exponential fluorescence decay (dash-dotted curve) according to $s_{F,\delta}(t) = x_{b,p} \exp(-t/\tau_{F,b,p,da}) + x_{b,ip} \exp(-t/\tau_{F,b,ip})$ (see Eq.S5) with $x_{b,p} = 0.901 \pm 0.02$, $\tau_{F,b,p,da} = 65 \pm 10$ ps, $x_{b,ip} = 0.099 \pm 0.02$, and $\tau_{F,b,ip} = 500 \pm 100$ ps. $x_{b,p}$ is the fraction of proper non-covalently bound flavin with average fluorescence lifetime $\tau_{F,b,p,da}$. $x_{b,ip}$ is the fraction of improper non-covalently bound flavin with fluorescence lifetime $\tau_{F,b,ip}$. The improper bound flavin is due to release of proper bound flavin in the BLUF domain signaling state (see below). The procedure of fluorescence component amplitude and fluorescence lifetime extraction by convolution fitting is explained in section S3 of the Supplementary material.

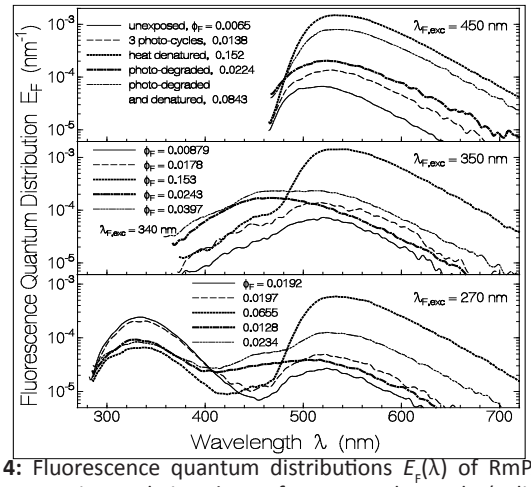

Figure 4: Fluorescence quantum distributions $E_F(\lambda)$ of RmPAE under different experimental situations of unexposed sample (solid curves), sample after three photo-cycles (dashed curves), fresh sample after heat-denaturation (dotted curves), sample after photo-degradation of Fig.10 (thick dash-dotted curve), and sample after photo-degradation and heat denaturing (dash-triple-dotted curves). Top part: fluorescence excitation wavelength $\lambda_{F,exc}$ = 450 nm. Middle part: $\lambda_{F,exc}$ = 350 nm except indicated differently. Bottom part: $\lambda_{F,exc}$ = 270 nm. The fluorescence quantum yields are listed in the legends.

In Fig.5b a fluorescence trace of the same RmPAE sample is shown which was measured with our ultrafast streak-camera system. The solid curve in the top part of Fig.5b shows the measured normalized fluorescence trace $S_{F,da}(t)/S_{F,da,max}$ (average of 10 measured traces, temperature ϑ = 21.1 °C). The dotted curve shows the approximate contribution of free flavin and improper bound flavin $[S_{F,free}(t) + S_{F,b,ip}(t)]/S_{F,da,max}$. The dashed gives the approximate contribution of the proper bound flavin $S_{F,da,b,p}(t)/S_{F,da,max}$. In the bottom part of Fig.5b a bi-exponential convolution fit of the proper bound flavin signal is presented. The solid curve is $S_{F,da,b,p}(t)/S_{F,da,b,p,max}$. The dotted curve is the system response function (measured by attenuating the excitation laser pulse and detecting it with the streak-camera). The dash-dotted curve shows the bi-exponential convolution fit curve (Eq.S3 and Eq.S5) with $x_{f,da} = 0.5$ (fraction of fast decaying excited flavin), $x_{sl,da} = 1 - x_{f,da} = 0.5$ (fraction of slow decaying excited flavin), $\tau_{F,f,da} = 5$ ps (fluorescence lifetime of fast component, determined by Tyr to excited flavin in receptor state Fl_r^* reductive electron transfer $Tyr + Fl_r^* \rightarrow Tyr^{\bullet+} + Fl_r^{\bullet-}$ [10,26]), and $\tau_{F,sl,da} = 78$ ps (fluorescence lifetime of slow component, determined by the $Fl_r^{\bullet-}$ state lifetime [10,26], see below).

The mean fluorescence lifetime of proper bound flavin in the dark adapted state is $\bar{\tau}_{F,b,p,da} = x_{f,da}\tau_{F,f,da} + x_{sl,da}\tau_{F,sl,da} \approx$ 41.5 ps. The fluorescence quantum yield of proper bound flavin in

the dark-adapted state is $\phi_{F,b,p,da} = \bar{\tau}_{F,b,p,da} / \tau_{rad,Fl}$ ≈ 2.2×10^{-3} using $\tau_{rad,Fl}$ ≈ 19 ns (value determined for riboflavin in aqueous solution [27]).

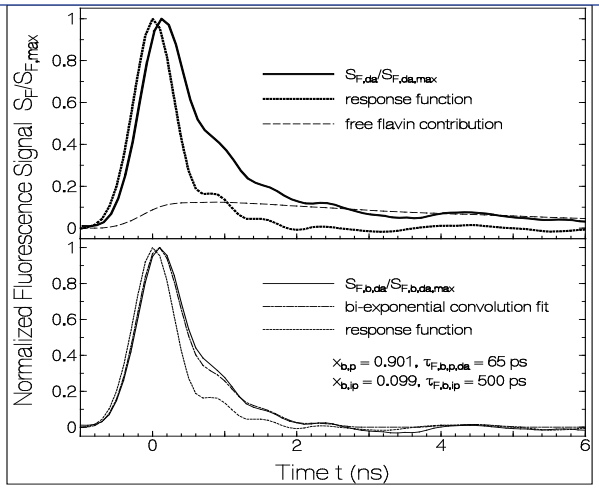

Figure 5a: Temporal fluorescence signal behavior of fresh unexposed RmPAE sample registered with microchannel-plate photomultiplier tube.

Top part: Solid curve: measured trace. Dotted curve: system response function. Dashed curve: convolution curve of free flavin fluorescence contribution.

Bottom part: Solid curve: experimental fluorescence trace deprived from free flavin contribution. Dotted curve: response function. Dash-dotted curve: Bi-exponential convolution fit (see main text).

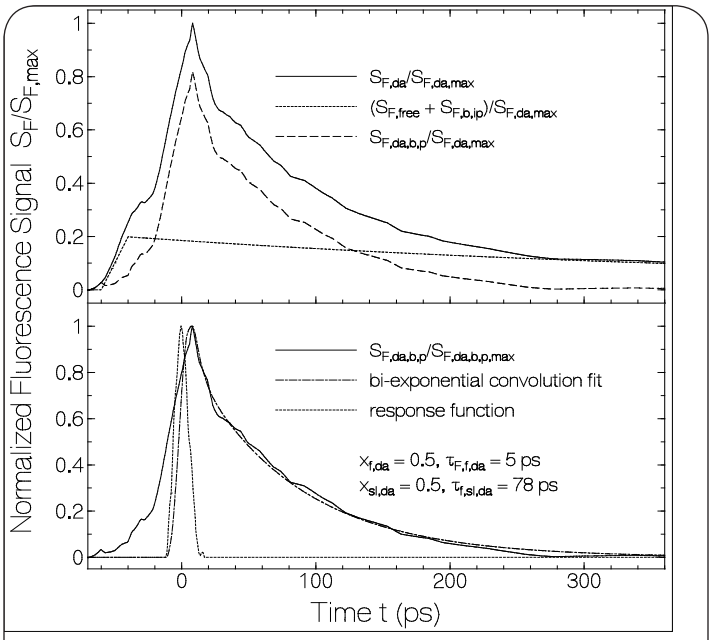

Figure 5b: Temporal fluorescence signal behavior of fresh unexposed dark-adapted RmPAE sample registered with the ultrafast streak-camera.

Top part: Solid curve: Normalized streak-camera trace. Dotted curve: approximate free flavin and improper bound flavin contribution. Dashed curve: approximate proper bound flavin contribution.

Bottom part: Solid curve: normalized proper bound flavin contribution. $S_{F,da,b,p}/S_{F,da,b,p,max}$. Dotted curve: system response function. Dash-dotted curve: bi-exponential convolution fit.

The fluorescence quantum yield of the non-covalently bound flavin in unexposed RmPAE $\phi_{F,b,da}$(flavin) is determined by subtracting the free flavin contribution from the total measured fluorescence quantum yield of dark adapted flavin, i.e $\phi_{F,b,da}(flavin) = \phi_{F,da}(flavin)\left(\int S_{F,da}(t)dt - \int S_{F,free}(t)dt\right)/\int S_{F,da}(t)dt$ ≈ 3.52×10^{-3} using $\phi_{F,da}$(flavin) = 0.0065 (solid curve in top part of Fig.4) and $\left(\int S_{F,da}(t)dt - \int S_{F,free}(t)dt\right)/\int S_{F,da}(t)dt$ ≈ 0.54 (integrals over solid curve and dashed curve in top part of Fig.5a). The fluorescence quantum yield contribution of the free flavin is $\phi_{F,free} = \phi_{F,da} - \phi_{F,b,da}$ = 0.00298. The fraction of free flavin $x_{Fl,free}$ is estimated by the relation $x_{Fl,free} \approx \phi_{F,free}/\phi_{F,denatured}$ giving $x_{Fl,free}$ ≈ 0.0196 using $\phi_{F,denatured}$ = 0.152 (see below).

Thermal investigations: Thermal investigations of RmPAE were carried out to get information on the thermal protein stability and to determine the flavin composition. The studies are given in the Supplementary material (section S4). The apparent RmPAE protein melting temperature ϑ_m was determined by stepwise sample heating and observing the vibronic structure of the first absorption band [14]. A value of ϑ_m = 63±2 °C was found. The flavin composition in RmPAE was determined by fluorescence quantum yield analysis after heat-denaturation (see dotted curves in Fig.4 and detailed presentations in Fig.S4 and Fig.S5). The mole-fraction of FMN (and possible riboflavin RF) turned out to be $x_{FMN,RF}$ = 0.604±0.015 and the mole-fraction of FAD was found to be $x_{FAD} = 1 - x_{FMN,RF}$ = 0.396±0.015.

Spectroscopic characterization of light exposed RmPAE

Absorption photo-cycling: The photo-cyclic absorption behavior of RmPAE was studied at room temperature. Attenuation spectra were measured before, during, and after light exposure.

In a first photo-cycling experiment a fresh centrifuged sample was exposed at 455 nm with I_{exc} = 0.0938 W cm^{-2} for a duration of 2.8 min (exposed input energy density $w_{exc,1}$ = 15.76 J cm^{-2}) at a temperature of ϑ = 23.8±0.2 °C. The solid curve in the top part of Fig.6 shows the attenuation coefficient spectrum of unexposed RmPAE (dark-adapted state). The dashed curve in the top part of Fig.6 shows the attenuation coefficient spectrum of RmPAE due to sample exposure at λ_{exc} = 455 nm with input excitation intensity of I_{exc} = 0.0938 W cm^{-2} at t_{exc} = 12 s. For this exposure time RmPAE is already practically completely converted to the signaling state (saturated light-adapted state). The S_0-S_1 flavin absorption band red shift in the signaling state is $\delta\lambda_{s,r}$ ≈ 5.4 nm.

In the bottom part of Fig.6 the absorption difference spectrum $\delta\alpha_{exc}(\lambda) = \alpha_{t_{exc}=12\,s}(\lambda) - \alpha_{unexposed}(\lambda)$ is displayed. The strongest absorption change due to signaling state formation occurred at $\lambda = \lambda_{\delta\alpha,max}$ = 482 nm.

The photo-cycling behavior of the same RmPAE sample in a second excitation - recovery cycle one day later is displayed in Fig.S6 of the Supplementary material (section S5.1). There the sample excitation intensity at λ_{exc} = 455 nm was I_{exc} = 0.938 mW cm^{-2} and the total duration of exposure was t_{exc} = 5.2 min. The RmPAE signaling state recovery was followed over 66.4 min. The top part of Fig.S6 displays the temporal signaling state formation, the middle part shows the signaling state recovery to the receptor state, and the lower part displays the absorption difference between dark recovered sample and initial sample.

In order to determine the efficiency of signaling state formation and the time constant of signaling-state recovery to the receptor state in the dark, the attenuation coefficient development at λ_{pr} = 482 nm was measured in a forth photo-cycling experiment (a third photo-cycling with λ_{exc} =455 nm, I_{exc} = 0.938 mW cm^{-2}, and t_{exc} = 5.8 min was carried for studies of the fluorescence development, see below). The initial absorption coefficient of the sample at 455 nm was $\alpha_{abs,initial}$(455 nm) = 1.635 cm^{-1} corresponding to $N_{0,Fl}$ = 3.97×10^{16} cm^{-3}. The sample was excited at λ_{exc} = 455 nm with I_{exc} = 0.938 mW cm^{-2} for t_{exc} = 225.65 s at ϑ = 24.7 °C. The attenuation coefficient development $\alpha_{482\ nm}(t)$ before light exposure, during light exposure, and after light exposure is shown in Fig.7. The main part of Fig.7 covers the time range from t = 0 to t = 7000 s. The inset gives an expanded view of the time range from t = 0 to t = 300 s. The dash-dotted curve in the main figure is a single exponential fit to the absorption recovery after excitation light switch of, i.e.

$$\alpha(\lambda_{pr},t_{rec}) = \alpha(\lambda_{pr},0) - \Delta\alpha(\lambda_{pr})\left[1-\exp\left(-t_{rec}/\tau_{rec}\right)\right]$$

with $\alpha(\lambda_{pr},0) = \alpha(\lambda_{pr},t_{exc,end})$ = 1.147 cm^{-1}, $\Delta\alpha(\lambda_{pr}) = \alpha(\lambda_{pr},t_{exc,end,}) - \alpha(\lambda_{pr},t_{exc,start})$ = 0.521 cm^{-1}, and τ_{rec} = 1146.3 s.

The quantum yield of signaling state formation ϕ_s is determined from the rise of absorption at λ_{pr} = 482 nm at the onset of light exposure (inset of Fig.7). ϕ_s is defined as the ratio of the increment of length-integrated number density ΔN_s of RmPAE BLUF domains converted to the signaling state to the corresponding increment of absorbed excitation photons $\Delta n_{ph,abs}$, i. e.

$$\phi_s = \frac{\Delta N_s}{\Delta n_{ph,abs}}. \qquad (1)$$

The increment of length-integrated number density ΔN_s is given by

$$\Delta N_s = N_{Fl,0}\ell_{exc}\frac{\Delta\alpha_{pr}}{\Delta\alpha_{pr,max}}, \qquad (2)$$

where $N_{Fl,0}$ is the initial number density of flavin, ℓ_{exc} is the sample length in excitation direction, $\Delta\alpha_{pr}$ is the absorption coefficient change at the probe wavelength λ_{pr} due the photon absorption $\Delta n_{ph,abs}$, and $\Delta\alpha_{pr,max}$ is the maximum absorption coefficient change at the probe wavelength λ_{pr} belonging to total conversion of RmPAE in the receptor state to RmPAE in the signaling state.

The increment of absorbed excitation photons $\Delta n_{ph,abs}$ at the onset of light exposure for duration t_{exc} is

$$\Delta n_{ph,abs} = \frac{I_{exc}t_{exc}}{h\nu_{exc}}\left[1-\exp\left(-\alpha_{da}(\lambda_{exc})\ell_{exc}\right)\right]. \qquad (3)$$

Using experimental parameters $\alpha_{da}(\lambda_{exc}) = \alpha_{da}$(455 nm) = 1.635 cm^{-1}. ℓ_{exc} = 0.15 cm, t_{exc} = 1.7 s, $\Delta\alpha_{pr}$ = 0.04424 cm^{-1}, $\Delta\alpha_{pr,max}$ = 0.534 cm^{-1}, I_{exc} = 9.38×10^{-4} W cm^{-2}, and $N_{0,Fl}$ = 3.97×10^{16} cm^{-3} we determine

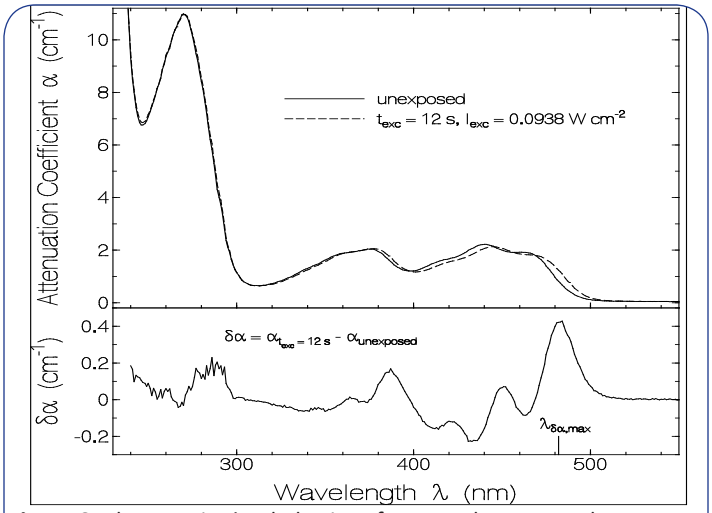

Figure 6: Photo-excitation behavior of RmPAE due to sample exposure at 455 nm. Temperature ϑ = 23.8 °C. Top part: Solid curve: attenuation coefficient spectrum α(λ) = α_{da}(λ) of unexposed sample (dark-adapted sample). Dashed curve: α(λ) = α_{la}(λ) of sample exposed at 455 nm for t_{exc} = 12 s with I_{exc} = 93.8 mW cm^{-2} (light adapted sample, RmPAE in signaling state). Bottom part: Attenuation coefficient difference spectrum δα(λ) = α_{la}(λ) - α_{da}(λ).

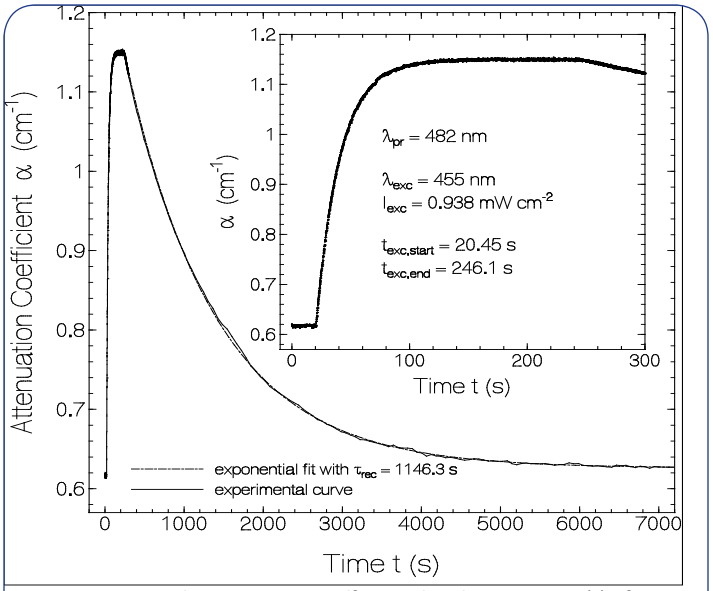

Figure 7: Temporal attenuation coefficient development $\alpha_{482}(t)$ of RmPAE before, during and after excitation at λ_{exc} = 455 nm with I_{exc} = 0.938 mW cm^{-2} (see main text).

$\Delta n_{ph,abs} = 7.938\times10^{14}$ cm^{-2} and $\Delta N_s = 4.728\times10^{14}$ cm^{-2}. Insertion of these values into Eq.1 gives a quantum yield of signaling state formation of $\phi_s = 0.596$.

After excitation light switch-off the attenuation coefficient at λ_{pr} = 482 nm recovered single exponentially from the signaling state value to the receptor state value with the time constant of τ_{rec}(24.7 °C) = 1146.3 s = 19.1 min (dash-dotted curve in main part of Fig.7).

The photo-cycling behavior of a further RmPAE sample was investigated at ϑ = 4.1±0.1 °C. The temporal attenuation coefficient development $\alpha(482\text{ nm}, t)$ is shown in Fig.S7 of the Supplementary material (section S5.1). The time constant of signaling state recovery to the receptor state was found to be τ_{rec}(4.1 °C) = 129 min.

The photo-excitation of flavin caused a protein conformational change from the receptor state to the signaling state. After light switch-off the protein recovered from the signaling state conformation back to the receptor state conformation via a potential energy activation barrier E_A. The recovery follows an Arrhenius relation according to [14,28]

$$\tau_{rec}(\vartheta) = \tau_{rec,0}\exp\left(\frac{E_A}{k_B\vartheta}\right) \approx \frac{h}{k_B\vartheta}\exp\left(\frac{E_A}{k_B\vartheta}\right), \quad (4)$$

where $\tau_{rec,0} \approx h/(k_B\vartheta)$ is the inverse attempt frequency of barrier crossing [14,29] and E_A is the activation barrier height. h is the Planck constant and k_B is the Boltzmann constant. Solving Eq.4 for E_A gives

$$E_A \approx k_B\vartheta\ln\left(\frac{\tau_{rec}(\vartheta)k_B\vartheta}{h}\right) \quad (5)$$

Insertion of parameters (τ_{rec} (297.85 K) = 1146.3 s and τ_{rec} (277.25 K) = 7740 s) gives E_A(297.85 K) ≈ 1.50×10^{-19} J ($\tilde{\nu}_A = E_A/(hc_0)$ ≈ 7551 cm^{-1}) and E_A(277.25 K) ≈ 1.47×10^{-19} J ($\tilde{\nu}_A = E_A/(hc_0)$ ≈ 7383 cm^{-1}). Within the experimental accuracy E_A is independent of the sample temperature ($\tilde{\nu}_A = E_A/(hc_0)$ ≈ 7470±100 cm^{-1}).

Fluorescence photo-cycling

Fluorescence emission spectroscopic behavior: The RmPAE sample used for the photo-cycle studies of Fig.6 and Fig.S6 was photo-excited a third time for fluorescence spectroscopic investigations at λ_{exc} = 455 nm with I_{exc} = 0.938 mW cm^{-2} for 5.8 min (first photo-cycle: I_{exc} = 0.0938 W cm^{-2} for 2.8 min, see Fig.6; second photo-cycle: I_{exc} = 0.938 mW cm^{-2} for 5.2 min, see Fig.S6).

The temporal development of the fluorescence quantum yield ϕ_F and of the fluorescence quantum distribution at λ = 480 nm E_F(480 nm) (there dominant emission of non-covalently bound flavin in the receptor state) is displayed in Fig.8. The top part shows the applied temporal excitation intensity. The middle part shows the fluorescence quantum yield before light exposure, at the end of light exposure (30 s after light switch-off) and its temporal evolution after light switch-off. The bottom part shows the development of E_F(480 nm) before light exposure, at the end of light exposure (30 s after light switch-off) and after light switch-off.

The fluorescence quantum yield ϕ_F of flavin in RmPAE decreased during light exposure since the efficiency of fluorescence emission of non-covalently bound flavin in the signaling state of RmPAE is less than that in the receptor state. After light switch-off the flavin fluorescence efficiency increased beyond the fluorescence efficiency before light exposure with a time constant of $\tau_{\phi_F,rec}$ = 12.91±0.3 min at ϑ = 24.5 °C which is shorter than the time constant τ_{rec} of absorption recovery. This behavior indicates a partial bound flavin rearrangement in the BLUF domain towards higher fluorescence efficiency (proper non-covalently bound flavin in the BLUF domain rearranged to improper non-covalently bound flavin during the signaling state lifetime, see below). The dependences are analyzed in the Supporting material (section S5.2).

The fluorescence quantum distribution E_F(480 nm) (bottom part of Fig.8) is determined by the fluorescence behavior of proper non-covalently bound flavin. This fluorescence quantum distribution decreased during light exposure and recovered approximately to the initial value before light exposure single exponentially with the time constant $\tau_{E_F(480\,nm)}$ = 21.34±3 min at ϑ = 24.5 °C.

The photo-cyclic fluorescence behavior of RmPAE will be explained below including the temporal fluorescence signal (lifetime) behavior as partial release of active non-covalently bound flavin in the BLUF domain to improperly bound flavin in the BLUF domain or to released flavin from the BLUF domain (kept in the RmPAE nano-cluster) during the stay of RmPAE in the signaling state.

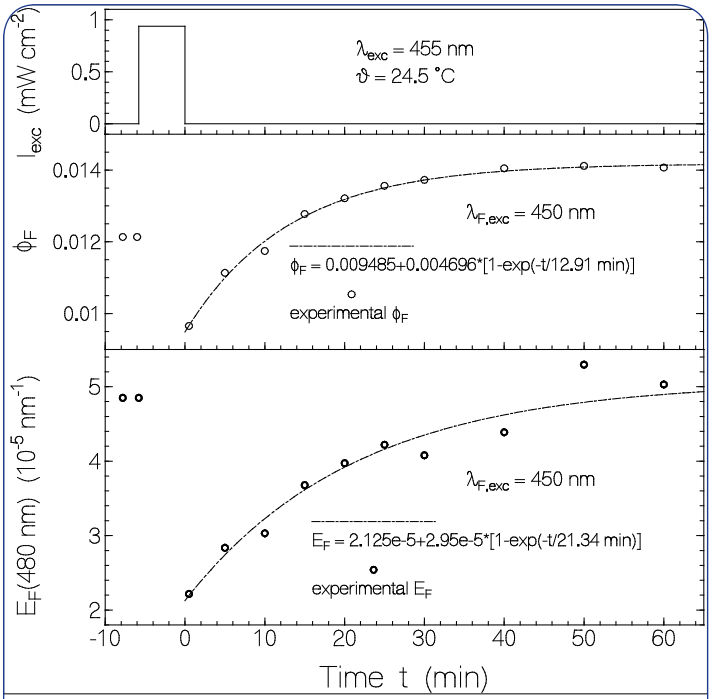

Figure 8: Photo-cycle dependence of flavin fluorescence emission. Third photo-cycle is considered. Top part: excitation intensity profile. Middle part: fluorescence quantum yield $\phi_F(t)$. Bottom part: fluorescence quantum distribution $E_F(480\text{ nm}, t)$.

Details of the fluorescence spectroscopic behavior of RmPAE due to photo-excitation to the signaling state are given in the Supplementary material section S5.2.

Fluorescence Lifetime Behavior: The fluorescence lifetime behavior of dark-adapted RmPAE was shown above in Fig.5a and 5b. The fluorescence lifetime behavior of RmPAE in the signaling state is displayed in Fig.9.

For recording fluorescence signal traces of RmPAE in the signaling state with our streak-camera system the sample was mounted in proper position before the streak-camera and it was excited laterally with our LED 455 nm light source (sample exposure with 0.8 mW cm^{-2} for 2 min immediately before fluorescence lifetime measurement, and exposure with I_{exc} = 63 µW cm^{-2} during fluorescence lifetime measurement). The sample temperature was ϑ = 21.1 °C. The fluorescence excitation occurred with picoseconds laser pulses of 1 ps duration, and 400 nm wavelength.

The solid curve in the top part of Fig.9 shows a recorded normalized fluorescence lifetime trace $S_{F,la}(t)/S_{F,la,max}$ (average of 10 measured single traces) of RmPAE in the signaling state. The dotted curve shows the approximate contribution of free flavin and improper bound flavin $[S_{F,free}(t)+ S_{F,b,ip}(t)]/S_{F,la,max}$. The dashed gives the approximate contribution of the proper bound flavin $S_{F,la,b,p}(t)/S_{F,la,max}$. In the bottom part of Fig.9 a bi-exponential convolution fit of the proper bound flavin signal in the signaling state is presented. The solid curve is $S_{F,la,b,p}(t)/S_{F,la,b,p,max}$. The dotted curve is the system response function (the same as in Fig.5b). The dash-dotted curve shows a bi-exponential convolution fit (Eq.S3 and Eq.S5) using

$$s_{F,la,b,p,\delta}(t) = x_{f,la}\exp\left(-t/\tau_{F,f,la}\right) + x_{sl,la}\exp\left(-t/\tau_{F,sl,la}\right)$$

with $x_{f,la}$ = 0.8, $x_{sl,la}$ = 1 – $x_{f,la}$ = 0.2, $\tau_{F,f,la}$ = 1.2 ps (electron transfer time from Tyr to Fl_s^* [10,26]), and $\tau_{F,sl,la}$ = 60 ps (Fl_s^* state lifetime) [10,26].

The mean fluorescence lifetime of proper bound flavin in the signaling state is $\bar{\tau}_{F,b,p,la} = x_{f,la}\tau_{F,f,la} + x_{sl,la}\tau_{F,sl,la}$ ≈ 13 ps. The fluorescence quantum yield of proper bound flavin in the light-adapted state is $\phi_{F,b,p,la} = \bar{\tau}_{F,b,p,la}/\tau_{rad,Fl}$ ≈ 6.8×10^{-4} using $\tau_{rad,Fl}$ ≈ 19 ns (value determined for riboflavin in aqueous solution [27]).

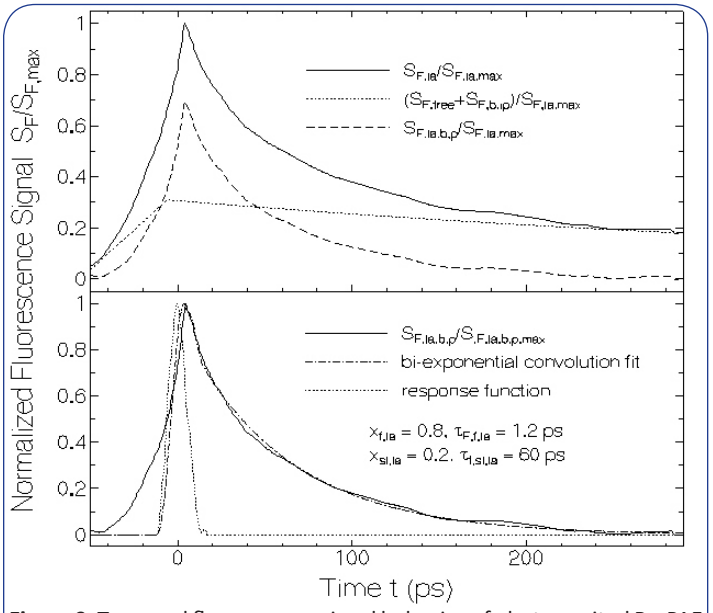

Figure 9: Temporal fluorescence signal behavior of photo-excited RmPAE sample (sample of Fig.5 is used).For details see main text. Top part: Solid curve: measured streak-camera trace. Dotted curve: fluorescence contribution of free flavin and improper bound flavin. Dashed curve: fluorescence contribution of proper bound flavin. Bottom part: Solid curve: normalized fluorescence signal of proper bound flavin. Dotted curve: system response function. Dash-dotted curve: bi-exponential convolution fit.

Photo-Degradation: The photo-degradation of RmPAE in the signaling state was studied by sample expose at λ_{exc} = 455 nm with an input intensity of I_{exc} = 0.108 W cm^{-2} over a time period of t_{exp} = 102.8 min. Thereby attenuation coefficient spectra were recorded at certain exposure times, and at the end of exposure the fluorescence spectral behavior was investigated. The sample temperature was ϑ = 23.8±0.5 °C.

In Fig.S11 of the Supplementary material (section S6) the measured attenuation coefficient spectra are displayed. In Fig.10 the corresponding absorption coefficient spectra are shown (scattering contribution approximately subtracted). The thick dotted curve in Fig.10 shows the absorption coefficient spectrum before light exposure (RmPAE in dark-adpted state). The thin solid curve belongs to an exposed input excitation energy density of w_{exc} = 1.125 J cm^{-2}. This curve shows the absorption coefficient

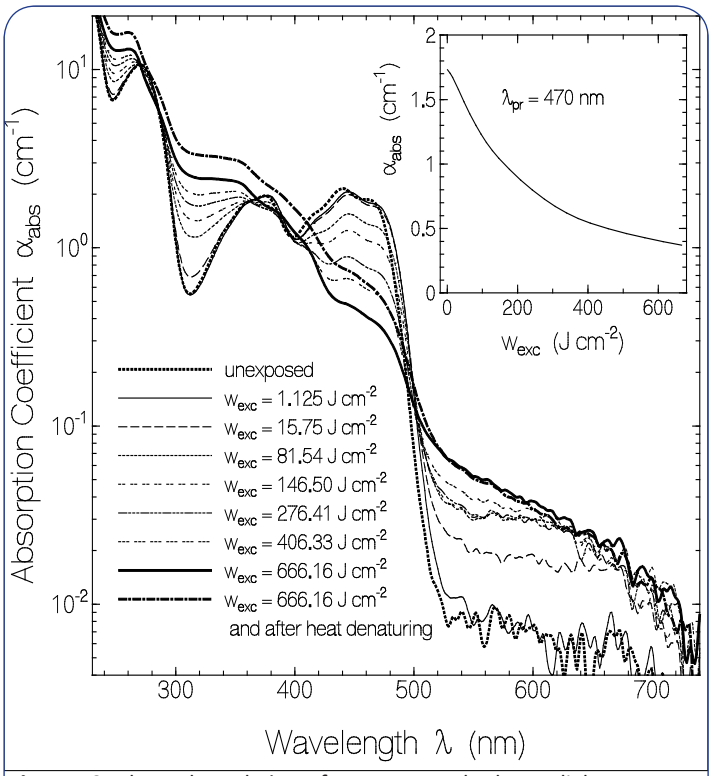

Figure 10: Photo-degradation of RmPAE sample due to light exposure at 455 nm. Accumulated exposed excitation energy density w_{exc} is listed in the legend. Absorption coefficient spectra are presented (scattering contribution is subtracted). Inset: absorption coefficient development $\alpha_{abs}(\lambda_{pr}$ = 470 nm) versus exposed excitation energy density w_{exc}.

spectrum of RmPAE in the signaling state. The other curves show the absorption coefficient spectra belonging to increasing exposed input energy densities. The absorption coefficient spectra are changed because of photo-degradation of RmPAE in the signaling state. The Fl_{ox} absorption decreased (absorption band around 450 nm). The inset in Fig.10 depicts the absorption coefficient development versus exposed excitation energy density at λ_{pr} = 470 nm where Fl_{ox} is dominantly absorbing.

The photo-degradation turned out to be irreversible. After excitation light switch-off the attenuation coefficient spectrum did not change (spectrum measured three days after light exposure before heat-denaturing, no change in attenuation coefficient spectrum was observed, curve not shown). After three days of storage of the photo-degraded sample in the dark at 4 °C, the sample was heat-denatured (insertion in heat bath at 66.3 °C and heating up to 85.6 °C within 10 min, then cooling down and centrifugation at 4 °C for 15 min with 4400 rpm). The resulting absorption coefficient spectrum is shown by the thick dash-dotted curve in Fig.10. The shape of the absorption coefficient spectrum after heat-denaturation is approximately the same as before heat-denaturation. Only the absorption strength increased somewhat (roughly a factor of 1.5) likely because of some solvent evaporation in the heating process.

The dominant RmPAE photoproduct likely consists of RmPAE apoprotein with covalently bound fully reduced flavin [10,30,31]. Non-covalently bound fully reduced flavin would be released from the protein in the process of protein heat denaturizing and then re-oxidized to Fl_{ox} [32] which is not observed. Likely fully reduced flavin is linked to the RmPAE protein by covalent binding to the tyrosine involved in the BLUF domain photo-cycle (Fl_{ox}* + TyrOH → $Fl^{\cdot-}$ + $TyrOH^{\cdot+}$, $Fl^{\cdot-}$ + $TyrOH^{\cdot+}$ → $FlH^{\cdot}$ + $TyrO^{\cdot}$, $FlH^{\cdot}$ + $TyrO^{\cdot}$ → FlH-OTyr [10,31]). The weak long-wavelength tail absorption (λ> 520 nm) may be due to a flavin – amino acid charge transfer complex [FlH^{-}…aa^{+}] (Fl_{ox}* + TyrOH + aa-H → $Fl^{\cdot-}$ + $TyrOH^{\cdot+}$ +aa-H →, [FlH^{-}…aa^{+}] + TyrOH) [33-35].

Fluorescence quantum distributions at $\lambda_{F,exc}$ = 450 nm, 350 nm and 270 nm after the photo-degradation are included in Fig.4 (thick dash-dotted curves). The curve belonging to $\lambda_{F,exc}$ = 450 nm shows that still some oxidized flavin Fl_{ox} is present. The curve belonging to $\lambda_{F,exc}$ = 350 nm indicates dominant lumichrome emission (peak around 460 nm) due to Fl_{ox} photo-degradation. The increased emission around 400 nm is attributed to some flavin degradation to quinoxalines (likely QO1 and QO4 of [23]). For $\lambda_{F,exc}$ = 270 nm fluorescence contributions from Tyr, quinoxalines (QO1, QO2, QO3, QO4 of [23]), lumichrome and oxidized flavin are seen. More fluorescence quantum distributions in the fluorescence excitation wavelength region from 230 nm to 480 nm are shown in Fig.S12.

Fluorescence quantum distributions at $\lambda_{F,exc}$ = 450 nm, 340 nm and 270 nm after photo-degradation and additional heat treatment for protein denaturation are included in Fig.4 (dashed-triple-dotted curves). The curve belonging to $\lambda_{F,exc}$ = 450 nm shows increased Fl_{ox} emission. The fluorescence quantum yield of fresh heat-denatured RmPAE is not reached because formed non-fluorescent adduct of RmPAE apoprotein and fully reduced flavin contributes to the absorption at $\lambda_{F,exc}$ = 450 nm. The curve belonging to $\lambda_{F,exc}$ = 340 nm indicates fluorescence contributions from oxidized flavin, lumichrome, and quinoxalines. For $\lambda_{F,exc}$ = 270 nm fluorescence contributions from Tyr, quinoxalines, lumichrome and oxidized flavin are seen. The fluorescence efficiency of Tyr and Fl_{ox} is reduced because of the dominant absorption of the non-fluorescent adduct of RmPAE apoprotein and fully reduced flavin at 270 nm. More fluorescence quantum distributions in the excitation wavelength region from 230 nm to 500 nm are shown in Fig.S13.

The initial quantum yield of flavin cofactor photo-degradation ϕ_D in the BLUF signaling state of RmPAE is estimated by analysis of the initial absorption decrease at 470 nm (Fig.10 with inset).

This quantum yield of photo-degradation ϕ_D is given by

$$\phi_D = \frac{\Delta N_{Fl_{ox,s}}}{\Delta n_{ph,abs}} \approx \frac{\Delta \alpha_{pr} / \sigma_{s,pr}}{\frac{\Delta w_{exc}}{h\nu_{exc}} \alpha_{exc}}. \qquad (6)$$

$\Delta N_{Fl_{ox,s}}$ is the number density of degraded flavins $Fl_{ox,s}$ in the signaling state due to the number density of absorbed excitation photons $\Delta n_{ph,abs}$. $\Delta\alpha_{pr}$ is the absorption coefficient decrease at λ_{pr} (470 nm), $\sigma_{s,pr}$ is the $Fl_{ox,s}$ absorption cross-section at λ_{pr}. Δw_{exc} is

the exposed excitation energy density at the start of light exposure, α_{exc} is the absorption coefficient of $Fl_{ox,s}$ at λ_{exc} (455 nm). Using the attenuation coefficient curves belonging to w_{exp} = 1.125 J cm^{-2} and w_{exp} = 15.75 J cm^{-2} (Δw_{exc} = 14.625 J cm^{-2}) of Fig.10 we get the parameters $\Delta\alpha_{Pr} \approx 0.0607$ cm^{-1}, $\sigma_{s,pr} \approx 3.72\times10^{-17}$ cm^2, $\alpha_{exc} \approx 1.89$ cm^{-1} and calculate $\phi_D \approx 2.58\times10^{-5}$. This low value of the quantum yield of photo-degradation of the flavin cofactor in the signaling state of the BLUF domain of RmPAE shows the high photo-stability of RmPAE.

Discussion

Results obtained by the spectroscopic characterization of RmPAE are collected in Table 1. The photo-cycling dynamics and the photo-degradation of RmPAE are discussed below.

In RmPAE the flavin loading factor was determined to be $\kappa_{Fl,load} \approx 0.26$ meaning that on the average four RmPAE apo-proteins share one flavin molecule. The RmPAE protein formed nano-clusters with an average cluster size of about 106 proteins aggregated together. A small fraction of $x_{Fl,free} \approx 0.02$ of flavins was found to be free. The flavin cofactor was found to consist of approximately 40 % FAD and 60 % FMN (and possibly riboflavin). The flavin non-covalently bound to the BLUF domain in fresh dark-adapted RmPAE, was in proper position for BLUF photo-cycling action (signaling state formation by blue light exposure, Fl positioned adjacent to Tyr for efficient photo-induced Tyr to flavin electron transfer). Blue-light photo-excitation caused signaling state formation (quantum yield of signaling state formation $\phi_s \approx 0.6$), and in the signaling state there occurred partial flavin repositioning (up to about 42 %) from BLUF active position to an improper BLUF inactive position with a time constant of re-localization of $\tau_{rel} \approx 40$ min at room temperature.

The fraction of flavin cofactor that took part in the position replacement from BLUF photo-cycle active site to inactive site in the signaling state was roughly equal to the mole-fraction of FAD in the flavin composition (χ_{FAD} = 0.396±0.015). It is thought that the FAD cofactor (larger size than FMN or riboflavin) suffers some force in the signaling state that cases some spatial re-positioning to negligible BLUF photo-cycling activity. The fluorescence lifetime of the improper bound flavin was determined to be $\tau_{F,b,ip}$ = 500±100 ps. It should be noticed that the fluorescence lifetime of FAD varies strongly with the arrangement of the isoalloxazine group and the adenine group of FAD [17,36,37] ($\tau_F \approx 7$ ps for stacked (closed) conformation [36] and $\tau_F \approx 3$ ns for un-stacked (stretched) conformation [17]).

A scheme of the RmPAE BLUF domain photo-cycle dynamics of proper bound flavin $Fl_{b,p}$ is displayed in Fig.11a ([38] and references therein). The photo-excitation of $Fl_{r,b,p}$ in the $BLUF_r$ receptor state to the first excited singlet state $Fl^*_{r,b,p}$ causes electron transfer from Tyr to $Fl^*_{r,b,p}$ ($TyrOH + Fl^*_{r,b,p} \rightarrow TyrOH^{\bullet+} + Fl^{\bullet-}_{r,b,p}$). During the $TyrOH^{\bullet+} - Fl^{\bullet-}_{r,b,p}$ radical ion-pair lifetime $\tau_{Fl^{\bullet-}_r} = \tau_{F,sl,da}$ there occurs a BLUF domain re-conformation with hydrogen bond restructuring to $BLUF_s$ [26] changing $TyrOH^{\bullet+} - Fl^{\bullet-}_{r,b,p}$ to $TyrOH^{\bullet+} - Fl^{\bullet-}_{s,b,p}$. The anionic flavin radical $Fl^{\bullet-}_{r,b,p}$ changes to $Fl^{\bullet-}_{s,b,p}$ with quantum efficiency ϕ_s and to $Fl_{r,b,p}$ with quantum efficiency 1 - ϕ_s. The time constant of signaling state formation is $\tau_{sf} = \tau_{Fl^{\bullet-}_r} / \phi_s$. The anionic flavin radical $Fl^{\bullet-}_{s,b,p}$ recovers to neutral $Fl_{s,b,p}$ with time constant $\tau_{Fl^{\bullet-}} = \tau_{F,sl,la} \approx \tau_{CR_s}$ according to $TyrOH^{\bullet+} + Fl^{\bullet-}_{s,b,p} \rightarrow TyrOH + Fl_{s,b,p}$.

In the $BLUF_s$ signaling state part of $Fl_{s,b,p}$ (likely $FAD_{s,b,p}$) is released with a time constant of τ_{rel} to $Fl_{b,ip}$ (likely $FAD_{b,ip}$). $BLUF_s$ recovered back to $BLUF_r$ with time constant τ_{rec} by thermal activated protein structure back re-conformation and hydrogen bond back restructuring (activation energy barrier E_A).

Photo-excitation of $Fl_{s,b,p}$ in the $BLUF_s$ signaling state caused faster Tyr to $Fl^*_{s,b,p}$ electron transfer (time constant $\tau_{F,f,la} = \tau_{ET,s}$) and charge recombination (time constant $\tau_{CR,s} \approx \tau_{F,sl,la}$) than photo-excitation of $Fl_{r,b,p}$ in the $BLUF_r$ receptor state. The flavin radical anion $Fl^{\bullet-}_{s,b,p}$

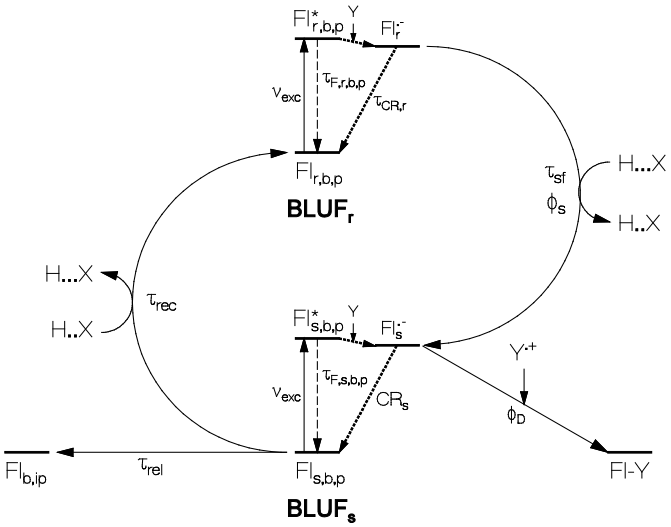

Figure 11a: Photo-cycling scheme of initially proper non-covalently bound flavin in $BLUF_r$ receptor state. (For details see main text).

and the tyrosine radical cation $TyrOH^{\bullet+}$ combined to the reduced flavin – tyrosine adduct FlH-OTyr (abbreviated Fl-Y in Fig.11a) approximately with the quantum yield of initial photo-degradation ϕ_D (for a detailed discussion see [10,31]).

The small amount of free flavin photo-degraded easily to lumichrome [16]. The absorption and emission spectroscopic studies of the RmPAE photo-degradation indicate that $Fl_{b,ip}$ and $Fl_{s,b,p}$ partly degrade with low quantum yield to lumichrome and other degradation products (likely including quinoxaline hydrolysis products of flavin [23]). For convenience structural formulae of fully oxidized flavin Fl_{ox}, lumichrome LC, reduced flavin – tyrosinyl adduct Fl-Tyr, and quinoxaline derivative QO1 (1,2-dihydro-2-keto-1,6,7-trimethyl-quinoxaline-3-carboxylic acid) are plotted in Fig.S14 of section S7 of the Supplementary material.

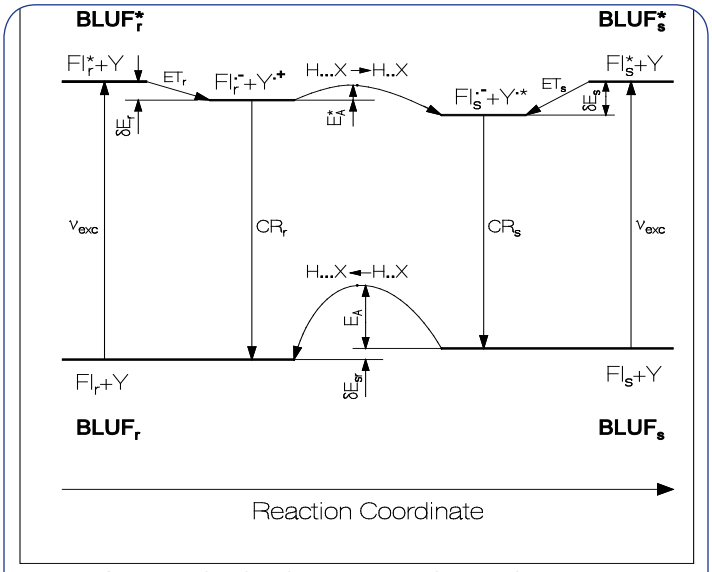

Figure 11b: Energy level and reaction coordinate scheme presentation of BLUF photo-cycle dynamics. (For details see main text).

In Fig.11b an energy level and reaction coordinate scheme of the BLUF photo-cycle dynamics is depicted. The left side shows the photo-excitation of $BLUF_r$ to $BLUF_r^*$ and the right side shows the photo-excitation of $BLUF_s$ to $BLUF_s^*$.

The excitation of $BLUF_r$ to $BLUF_r^*$ ($Fl_r + Y \xrightarrow{h\nu_{exc}} Fl_r^* + Y$) is followed by excited-state electron transfer ($Fl_r^* + Y \xrightarrow{ET_r} Fl_r^{\bullet-} + Y^{\bullet+}$) with electron transfer time constant $\tau_{ET_r} = \tau_{F,f,da}$. The energy difference δE_r between $Fl_r^* + Y$ and $Fl_r^{\bullet-} + Y^{\bullet+}$ determines the thermodynamic equilibrium between $Fl_r^* + Y$ and $Fl_r^{\bullet-} + Y^{\bullet+}$ and causes the bi-exponential fluorescence decay out of level Fl_r^* given by

$$S_{F,r}(t) = S_{F,r,0}[x_{f,da}\exp(-\frac{t}{\tau_{F,f,da}}) + x_{sl,da}\exp(-\frac{t}{\tau_{F,sl,da}})], \quad (7a)$$

with $x_{f,da} + x_{sl,da} = 1$ and

$$x_{sl,da} = \frac{\exp\left(-\frac{\delta E_r}{k_B\vartheta}\right)}{1+\exp\left(-\frac{\delta E_r}{k_B\vartheta}\right)}. \quad (7b)$$

Solving Eq.7b for the energy level difference δE_r gives

$$\delta E_r = -k_B\vartheta \ln\left(\frac{x_{sl,da}}{1-x_{sl,da}}\right) \quad (7c)$$

Insertion of parameters (Fig.5b, $x_{sl,da} \approx 0.5$, $\vartheta = 294.25$ K) gives $\delta E_r \approx 0$.

Similarly the energy difference δE_s between $Fl^*_s + Y$ and $Fl_s^{\bullet-} + Y^{\bullet+}$ is determined using Eqs.7a-7c by replacing subscript da by subscript la. Insertion of parameters (Fig.9, $x_{sl,la} \approx 0.2$, $\vartheta = 294.25$ K) gives $\delta E_s \approx 5.63\times10^{-21}$ J ($\delta\tilde{\nu}_s = \delta E_s/(hc_0) \approx 283$ cm^{-1}).

The activation energy barrier E_A of ground-state $BLUF_s$ recovery to ground-state $BLUF_r$ was determined above (Eqs. 4 and 5) to be $E_A \approx 1.49\times10^{-19}$ J ($\tilde{\nu}_A = E_A/(hc_0) \approx 7470$ cm^{-1}). Similarly, the activation barrier E_A^* of excited-state $BLUF_r^*$ transfer to $BLUF_s^*$ may be determined by the time constant τ_{sf} of photo-induced signaling state formation and the inverse attempt frequency of barrier crossing $\tau_{sf,0} \approx h/(k_B\vartheta)$ [14,29]. The responsible Arrhenius relation is

$$\tau_{sf}(\vartheta) = \tau_{sf,0}\exp\left(\frac{E_A^*}{k_B\vartheta}\right) \approx \frac{h}{k_B\vartheta}\exp\left(\frac{E_A^*}{k_B\vartheta}\right) \quad (8)$$

Using $\tau_{sf} = \tau_{F,sl,da}/\phi_s = 131$ ps ($\tau_{F,sl,da} = 78$ ps, $\phi_s = 0.596$), and $\vartheta = 21.1$ °C = 294.25 K one gets $E_A^* = k_B\vartheta\ln(\tau_{sf}k_B\vartheta/h) = 2.72\times10^{-20}$ J ($\tilde{\nu}_A^* = E_A^*/(hc_0) = 1367$ cm^{-1}).

The energy difference δE_{sr} between the ground-state energy levels Fl_s+Y of $BLUF_s$ and Fl_r+Y of $BLUF_r$ determines the fractions of flavin in the signaling state $x_{s,th}$ and in the receptor state $x_{r,th}$ under dark-adapted conditions at temperature ϑ according to

$$\frac{x_{s,th}}{x_{r,th}} = \frac{x_{s,th}}{1-x_{s,th}} = \exp\left(-\frac{\delta E_{sr}}{k_B\vartheta}\right). \quad (9a)$$

Solving for δE_{sr} gives

$$\delta E_{sr} = -k_B\vartheta\ln\left(\frac{x_{s,th}}{1-x_{s,th}}\right). \quad (9b)$$

An upper limit of $x_{s,th}$ is determined by the attenuation coefficient ratio of dark-adapted sample $\alpha_{da}(\lambda_{\delta\alpha,max})$ to light adapted sample $\alpha_{la}(\lambda_{\delta\alpha,max})$ at the wavelength position $\lambda_{\delta\alpha,max}$ of maximum absorption change between signaling state and receptor state (see Fig.6), i.e. $x_{s,th,\,upper\,limit} = \alpha_{da}(\lambda_{\delta\alpha,max})/\alpha_{la}(\lambda_{\delta\alpha,max})$. This upper limit determination assumes that the attenuation coefficient of RmPAE in the receptor state at $\lambda_{\delta a,max}$ is zero (i.e. $\alpha_{BLUFr}(\lambda_{\delta\alpha,max}) = 0$). From the bottom part of Fig.6 we obtain $\lambda_{\delta a,max} = 482$ nm and from the top part of Fig.6 we obtain $x_{s,th,\,upper\,limit} = 0.659$. Insertion of $x_{s,th,\,upper\,limit}$ into Eq.9b gives $\delta E_{sr} \geq 2.68\times10^{-21}$ J ($\delta\tilde{\nu}_{sr} = \delta E_{sr}/(hc_0) \geq 135$ cm^{-1}).

Table 1: Parameters of RmPAE in aqueous solution at pH 7.5 (10 mM NaH_2PO_4/Na_2HPO_4, 10 mM NaCl, 25 % glycerol).

Parameter	Value	Comments
$\chi_{FMN,RF}$	0.604±0.015	Fig.S5
χ_{FAD}	0.396±0.015	$\chi_{FAD} = 1-\chi_{FMN,RF}$
$\kappa_{Fl,load}$	0.26±0.03	Fig.3
ϑ_m (°C)	63±2	Fig.S3
$x_{Fl,free}$	0.0196 ±0.002	Fig.5a
$\tau_{F,Fl,free}$ (ns)	≈ 5.0	Fig.5a
$\phi_{F,Fl,da}$	0.0065±0.0005	Fig.S2, fresh sample
$\tau_{F,f,da}$ (ps)	5±1	Fig.5b, $\tau_{F,f,da} = \tau_{ET,r}$
$\tau_{F,sl,da}$ (ps)	78±5	Fig.5b, $x_{F,sl,da} = x_{CR,r}(1 - z_S)$
$x_{f,da}$	0.5±0.1	Fig.5b
$x_{,sl,da}$	0.5±0.1	Fig.5b
$\bar{\tau}_{F,b,p,da}$ (ps)	≈ 41.5	$x_{f,da}x_{F,f,da} + x_{sl,da}x_{F,sl,da}$
$\phi_{F,b,p,da}$	≈ 2.2×10^{-3}	$\phi_{F,b,p,da} = \bar{\tau}_{F,b,p,da} / \tau_{rad,Fl}$
$\tau_{F,b,ip}$ (ps)	500±100	Fig.5a
$\tau_{F,f,la}$ (ps)	1.2±0.2	Fig.9, $\tau_{F,f,la} = \tau_{ET,s}$
$\tau_{F,sl,la}$ (ps)	60±5	Fig.9, $\tau_{F,sl,la} \cdot \tau_{CR,s}$
$\bar{\tau}_{F,b,p,da}$(ps)	≈ 13	$x_{f,la}x_{F,f,la} + x_{sl,la}x_{F,sl,la}$
$\phi_{F,b,p,la}$	≈ 6.8×10^{-4}	$\phi_{F,b,p,la} = \bar{\tau}_{F,b,p,la} / \tau_{rad,Fl}$
$\tau_{rad,Fl}$ (ns)	≈ 19	[27]
$\delta\lambda_{s,r}$ (nm)	5.4±0.4	Fig.6
τ_{sf} (ps)	≈ 131	$x_{sf} = x_{F,sl,da} / z_s$
τ_{rec} (min)	19.1±0.5	Fig.7, ϑ = 24.7 °C
τ_{rel} (min)	39.8±2	Fig.8, Eq.S9b, ϑ = 24.5 °C
I_{sat} (W cm^{-2})	1.56×10^{-5}	Eq.S8b, ϑ = 24.7 °C
ϕ_s	0.596±0.04	Eqs.1-3
ϕ_D	≈ 2.58×10^{-5}	Eq. 6
$E_A/(hc_0)$ (cm^{-1})	7470±100	Eq.5
$E_A^*/(hc_0)$ (cm^{-1})	1367±50	Fig.11b, Eq.8
$\delta E_r/(hc_0)$ (cm^{-1})	≈ 0	Fig.11b, Eq.7c
$\delta E_s/(hc_0)$ (cm^{-1})	≈ 283±20	Fig.11b, analog Eq.7c
$\delta E_{sr}/(hc_0)$ (cm^{-1})	≥ 135	Fig.11b, Eq.9b

Abbreviations used in Table 1: $\chi_{FMN,RF}$ = fraction of FMN and riboflavin non-covalently bound in RmPAE. χ_{FAD} = fraction of FAD non-covalently bound in RmPAE. $\kappa_{Fl,load}$ = flavin loading of RmPAE. ϑ_m = apparent protein melting temperature. $x_{Fl,free}$ = mole fraction of free flavin. $\tau_{F,Fl,free}$ = fluorescence lifetime of free flavin. $\phi_{F,Fl,da}$ = complete fluorescence quantum yield of flavin in fresh dark-adapted state. $\tau_{F,f,da}$ = fast fluorescence lifetime of proper bound flavin in dark-adapted BLUF domain. $\tau_{F,sl,da}$ = slow fluorescence lifetime of proper bound flavin in dark-adapted BLUF domain. $x_{f,da}$ = fraction of flavins with fast fluorescence decay in dark-adapted state. $x_{sl,da}$ = fraction of flavins with slow fluorescence decay in dark-adapted state. $\bar{\tau}_{F,b,p,da}$ = mean fluorescence lifetime of proper bound flavin in dark-adapted state. $\phi_{F,b,p,da}$ = fluorescence quantum yield of proper non-covalently bound flavin in the dark-adapted state. $\tau_{F,b,ip}$ = fluorescence lifetime of improper non-covalently bound flavin. $\tau_{F,f,la}$ = fast fluorescence lifetime of proper bound flavin in light-adapted BLUF domain. $\tau_{F,sl,la}$ = slow fluorescence lifetime of proper bound flavin in light-adapted BLUF domain. $x_{f,la}$ = fraction of flavins with fast fluorescence decay in light-adapted state. $x_{sl,la}$ = fraction of flavins with slow fluorescence decay in light-adapted state. $\bar{\tau}_{F,b,p,da}$ = mean fluorescence lifetime of proper bound flavin in light-adapted state. $\phi_{F,b,p,la}$ = fluorescence quantum yield of proper non-covalently bound flavin in the light-adapted state. $\tau_{rad,Fl}$ = radiative lifetime of flavin (value determined for riboflavin is used [27]). $\delta\lambda_{s,r}$ = red-shift of S_0-S_1 absorption band due to signaling state formation. τ_{rec} = signaling state recovery time of RmPAE. τ_{rel} = time constant of flavin release from proper non-covalently bound position in BLUF domain of RmPAE during presence in the signaling state. I_{sat} = saturation intensity of signaling state formation for RmPAE. ϕ_s = quantum efficiency of signaling state formation. ϕ_D = quantum yield of RmPAE photo-degradation. E_A = activation barrier for thermal signaling state to receptor state recovery of RmPAE. E_A^* = activation barrier for signaling state formation in the excited state. δE_r = energy difference between $Fl_r^* + Tyr$ and $Fl_r^{\bullet-} + Tyr^{\bullet+}$. δE_s = energy difference between $Fl_s^* + Tyr$ and $Fl_s^{\bullet-} + Tyr^{\bullet+}$. δE_{sr} = energy difference between $Fl_s + Tyr$ and $Fl_r + Tyr$ in the ground-state.

Conclusions

The photodynamics of the engineered triple-mutated photoactivated endonuclease RmPAE from the mesophilic, pigmented bacterium *R. mesophilum* strain MSL-20^T was characterized by optical spectroscopic methods. The RmPAE BLUF domain photo-cycling efficiency of receptor state to signaling state conversion was found to be reasonably high (quantum yield of signaling state formation $\phi_s \approx 0.6$). The first absorption band spectral red-shift of the flavin cofactor in the signaling state was rather small ($\delta\lambda_{s,r} \approx 5.4$ nm). The RmPAE signaling-state conformation at room temperature recovered only slowly to the receptor state conformation (recovery time $\tau_{rec} \approx 19$ min). Because of the slow signaling state recovery, weak continuous blue light is sufficient to keep RmPAE in the saturated light-adapted state (saturation intensity at $\lambda_{exc} = 455$ nm is $I_{sat} \approx 16$ μW cm^{-2}, see section S5.1 of Supplmentary material). In the signaling state part of the flavin cofactor (likely FAD) at room temperature lost its photo-cycling activity with a time constant of $\tau_{rel} \approx 40$ min likely by re-localization to an electron-transfer inactive site. The thermal stability of RmPAE turned out to be reasonably high (apparent protein melting temperature of $\vartheta_m \approx 63$ °C) allowing convenient stable experimentation at room temperature.

The primary BLUF domain photo-cycling behavior of RmPAE starting from the BLUF domain in its receptor state ($BLUF_r$) was similar to other BLUF proteins studied thus far [38]. The first flavin absorption band spectral red-shift in the signaling state was rather small, and the signaling state recovery to the receptor state after light switch-off was rather long. Different to other BLUF proteins, for RmPAE in the signaling state, there occurred partial removal of BLUF active flavin in proper bound position to BLUF inactive flavin in improper position (likely FAD cofactor deactivation).

Photo-excitation of RmPAE in its light-adapted signaling state ($BLUF_s$, secondary BLUF domain photo-cycling) caused permanent flavin cofactor degradation with low quantum yield of photo-degradation partly to FlH-OTyr adduct formation and partly to conversion of flavin to lumichrome and quinoxaline derivatives. A similar secondary photo-cycling dynamics with FlH-OTyr adduct formation was observed for the photoactivated adenylyl cyclase LiPAC from the spirochete bacterium *Leptonema illini* strain 3055^T [10] and the photoactivated adenylyl cyclase TpPAC from the spirochete bacterium *Turneriella parva* strain H^T [31].

Acknowledgements

A. P. thanks Prof. F. J. Gießibl, University of Regensburg, for his kind hospitality. Madhu Bhagel is acknowledged for the initial bioinformatics analysis of the used gene. This work was partly supported by DST-JNU purse grant.

Supplementary Material to Photodynamics of photo-activated BLUF coupled Endonuclease III mutant RmPAE from mesophilic, pigmented bacterium *Rubellimicrobium mesophilum* strain MSL-20T

S1. Nano-cluster size of fresh dark-adapted RmPAE

The nano-cluster size of fresh dark-adapted RmPAE is determined analogous to the description in [20].

The scattering cross-section σ_{sca} is obtained from the scattering coefficient α_{sca} by $\sigma_{sca} = \alpha_{sca}/N_{RmPAE\ apoprotein}$. For the situation of Fig.3, in the transparency region at $\lambda = 632.8$ nm it is $\alpha_{sca}(\lambda) = \alpha_{sca}(\lambda_0)(\lambda_0/\lambda)^\gamma = 0.0166$ cm^{-1} ($\lambda_0 = 800$ nm,

$\alpha_{sca}(\lambda_0)$ = 0.0065 cm^{-1}, and γ = 4) and $\sigma_{sca}(\lambda)$ = 8.97×10^{-20} cm^2 ($N_{\text{RmPAE apoprotein}}$ = 1.85×10^{17} cm^{-3}).

The scattering cross-section is given by [39]

$$\sigma_{sca} = \beta_m \tilde{M} \sigma_{R,m}, \tag{S1}$$

with the monomer Rayleigh scattering cross-section

$$\sigma_{R,m} = \frac{8\pi}{3}\frac{4\pi^2 n_s^4}{\lambda^4} V_m^2 \left(\frac{n_{pr}^2 - n_s^2}{n_{pr}^2 + 2n_s^2}\right)^2 = \frac{8\pi}{3}\frac{4\pi^2 n_s^4}{\lambda^4}\left(\frac{M_{pr}}{N_A \rho_{pr}}\right)^2 \left(\frac{n_{pr}^2 - n_s^2}{n_{pr}^2 + 2n_s^2}\right)^2 \tag{S2}$$

Thereby β_m is the degree of aggregation (average number of protein molecules per cluster particle), and $\tilde{M}$ is the total Mie scattering function ($\tilde{M} \leq 1$ decreasing with increasing aggregate size [39]). n_s is the refractive index of the solvent (water buffer) at wavelength λ, n_{pr} the refractive index of the protein at wavelength λ, $V_m = M_{pr}/(N_A \rho_{pr})$ is the volume of one protein molecule, M_{pr} is the molar mass of the protein monomer (M_{pr} = 24781.959 g mol^{-1} for RmPAE apoprotein), N_A = 6.022142×10^{23} mol^{-1} is the Avogadro constant, and ρ_{pr} is the mass density of the protein (typical value for proteins is $\rho_{pr} \approx$ 1.412 g cm^{-3} [40]). These numbers give a protein monomer volume of $V_m \approx$ 29.14 nm^3 and a protein monomer radius of $a_m = [3V_m/(4\pi)]^{1/3} \approx$ 1.91 nm. At λ = 632.8 nm there is n_s = 1.332 and $n_{pr} \approx$ 1.589 [41] giving $\sigma_{R,m}$(632.8 nm) = 8.426×10^{-22} cm^2. Insertion into Eq.S1 gives $\beta_m \tilde{M} \approx \beta_m = \sigma_{sca}/\sigma_{R,m} \approx 106$. The average aggregate volume is $V_{ag} = \beta_m V_m \approx$ 3089 nm^3 and the average aggregate radius is $a_{ag} = \beta_m^{1/3} a_m \approx$ 9.04 nm (for this size Rayleigh scattering applies and $\tilde{M} = 1$ [39]).

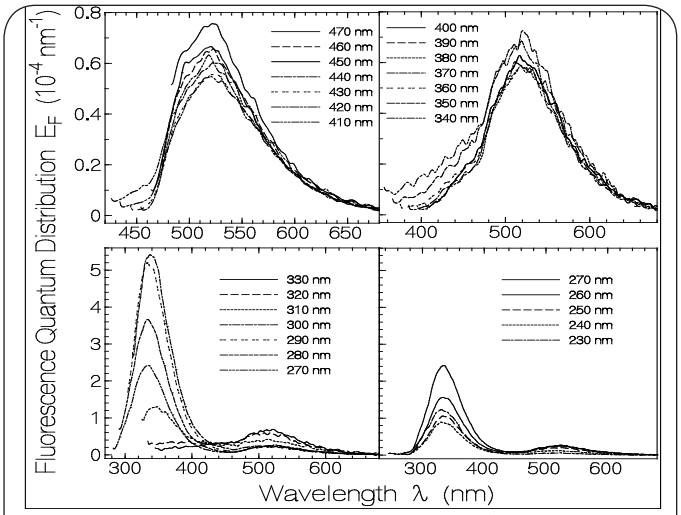

Fig.S1: Fluorescence quantum distributions $E_F(\lambda)$ of fresh dark-adapted RmPAE for different fluorescence excitation wavelengths in the range from $\lambda_{F,exc}$ = 470 nm to 230 nm.

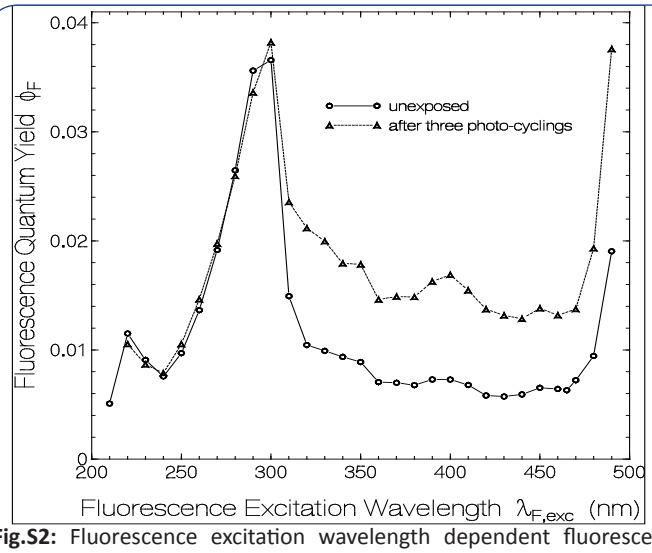

Fig.S2: Fluorescence excitation wavelength dependent fluorescence quantum yield ϕ_F of fresh dark-adapted RmPAE (circles) and of RmPAE after three photo-cycles (triangles).

S2. Fluorescence excitation wavelength dependent fluorescence emission of unexposed RmPAE

In Fig.S1 fluorescence quantum distributions $E_F(\lambda)$ of the unexposed centrifuged (4400 rpm, 15 min) RmPAE sample used in the absorption measurements of Fig.3 are presented for fluorescence excitation in the range from $\lambda_{F,exc}$ = 470 nm to 230 nm in steps of 10 nm. The dependence of the overall fluorescence quantum yield ϕ_F on $\lambda_{F,exc}$ is shown by the solid curve in Fig.S2.

S3. Fluorescence amplitude contribution and fluorescence lifetime determination by fluorescence trace convolution fit

Experimental normalized fluorescence traces $s_F(t) = S_F(t)/S_{F,max}$ are the convolution of the true δ-function pulse excitation fluorescence decay curve $s_{F,\delta}(t)$ and the system response function $g(t)$ according to [27]

$$s_F(t) = \frac{\int_{-\infty}^{t} g(t') s_{F,\delta}(t-t')dt'}{\max\left(\int_{-\infty}^{t''} g(t') s_{F,\delta}(t''-t')dt'\right)}, \tag{S3}$$

(the denominator with $-\infty < t'' < +\infty$ gives the normalization to $\max(s_F(t)) = 1$). For single exponential fluorescence decay $s_{F,\delta}(t)$ is given by

$$s_{F,\delta}(t) = \begin{cases} \exp\left(-\frac{t}{\tau_F}\right) & \text{for } t \geq 0 \\ 0 & \text{for } t < 0 \end{cases}, \tag{S4}$$

where τ_F is the fluorescence lifetime. In the determination of the fluorescence lifetime $\tau_{F,fit}$ values are inserted in Eq.S4, and $s_{F,fit}(t)$ curves are calculated by use of Eq.S3. $s_{F,fit}(t)$ is compared with the experimental $s_F(t)$. $\tau_{F,fit}$ agrees with the experimental τ_F when $s_{F,fit}(t)$ agrees with $s_F(t)$.

For two-component single-exponential fluorescence decay $s_{F,\delta}(t)$ is given by

$$s_{F,\delta}(t) = \begin{cases} x_1 \exp\left(-\frac{t}{\tau_{F,1}}\right) + (1-x_1)\exp\left(-\frac{t}{\tau_{F,2}}\right) & \text{for } t \geq 0 \\ 0 & \text{for } t < 0 \end{cases} \quad \text{(S5)}$$

x_1, $\tau_{F,1}$ and $\tau_{F,2}$ are adjusted to obtain a good fit of Eq.S3 to the experimentally measured fluorescence trace.

S4. Thermal investigations of fresh dark adapted RmPAE

The thermal protein stability was studied by stepwise sample heating up to 85.2 °C, then cooling down, thereby measuring the attenuation coefficient spectra development, and fluorescence characterization after the heating – cooling cycle. The apparent RmPAE protein melting temperature is derived from the loss of the vibronic structure of the S_0-S_1 absorption band of the flavin cofactor in RmPAE with sample heating [15]. The flavin composition (content of flavin-mononucleotide FMN, possible riboflavin, and flavin-adenine-dinucleotide FAD [42]) is estimated from fluorescence quantum yields measured after protein denaturing.

The heating-cooling temperature profile applied to the RmPAE sample used in the thermal investigations is displayed by the right inset of Fig.S3.

The main part of Fig.S3 shows attenuation coefficient spectra of RmPAE measured at selected temperatures during the sample heating up (19.5 °C start, 54.8 °C, 60.1 °C, 65.4 °C, 70.6 °C, 74.8 °C, 85.2 °C), cooling down (25 °C cooling down, dashed curve) and at the end of the sample cooling down and centrifugation (4 °C, end, dotted curve). The temperatures belonging to the curves are written to the curves. With rising temperature the light scattering increased (see increasing attenuation coefficient spectra) and the spectral structure of the S_0-S_1 absorption band of flavin (wavelength region from 400 nm to 500 nm) smoothed out. In cooling down the attenuation spectrum continued to increase. Only due to centrifugation the scattering reduced (dotted curve belonging to end of heating-cooling cycle with centrifugation at 4 °C). The final flavin absorption coefficient at the end of the heating-cooling cycle is higher than at the start of the heating-cooling cycle since some buffer solvent evaporated at the applied high temperatures (final sample volume less than initial sample volume).

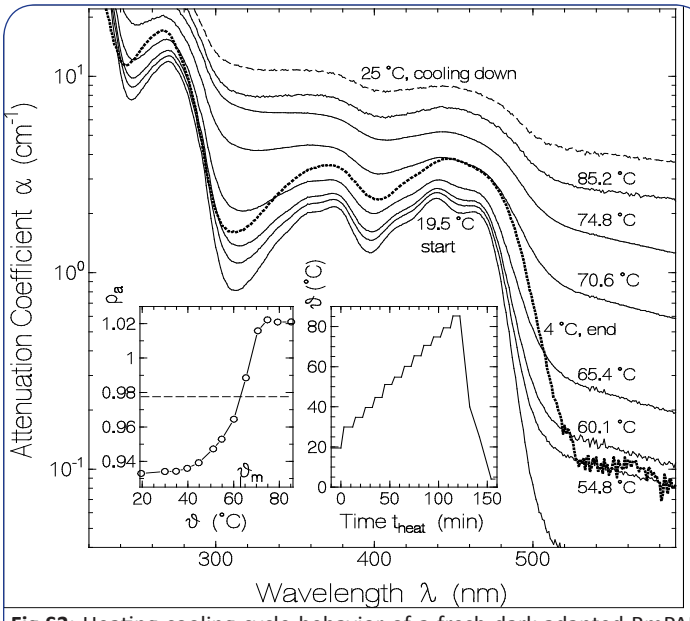

Fig.S3: Heating-cooling cycle behavior of a fresh dark-adapted RmPAE sample.

Main figure: Attenuation coefficient spectra α(λ) development during stepwise sample heating up and cooling down.

Right inset: Applied heating and cooling profile.
Left inset: $\rho_a(\vartheta)$ and $\rho_{a,mean}$. At apparent protein melting temperature ϑ_m it is $\rho_a(\vartheta) = \rho_{a,mean}$.

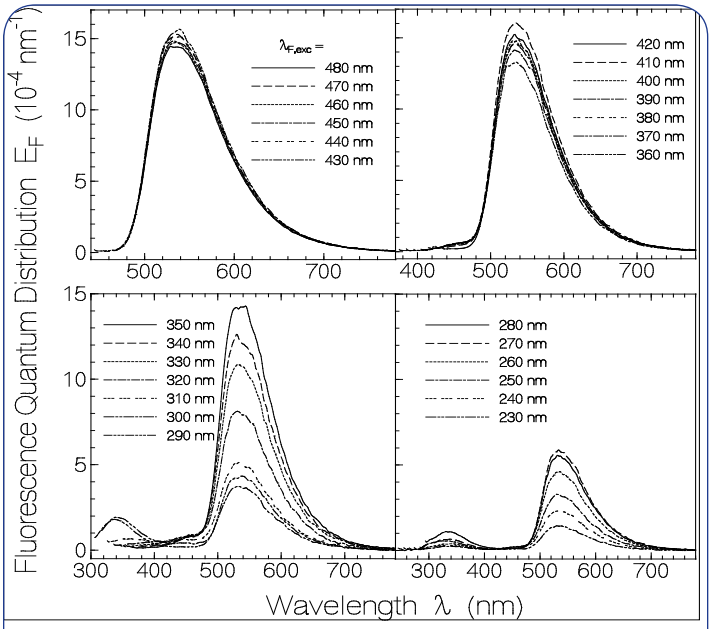

Fig.S4: Fluorescence quantum distributions $E_F(\lambda)$ of RmPAE after heat denaturing for various fluorescence excitation wavelength in the range from 230 nm to 480 nm.

The left inset of Fig.S3 shows the loss of the dip in the attenuation spectrum at λ = 455 nm with rising temperature due to protein denaturing (protein unfolding). The ratio $\rho_a(\vartheta) = 2\alpha(455\ nm, \vartheta)/[\alpha(440\ nm, \vartheta) + \alpha(462\ nm, \vartheta)]$ is displayed (line-connected circles). The dashed line is given by $\rho_{a,mean} = [\rho_a(19.5^oC) + \rho_a(85.2^oC)]/2$. The apparent RmPAE melting temperature ϑ_m is defined by $\rho_a(\vartheta_m) = \rho_{a,mean}$. A value of ϑ_m = 63±2 °C is determined.

The fluorescence emission quantum distributions of RmPAE after the heating-cooling cycle are shown in Fig.S4 for fluorescence excitation wavelengths in the range from $\lambda_{F,exc}$ = 480 nm to 230 nm in steps of 10 nm. The flavin fluorescence peaking around 535 nm is strongly increased compared to dark-adapted unheated RmPAE

(Fig.S1) due to flavin release from the protein. The Trp fluorescence peaking around 340 nm is decreased compared to the dark-adapted unheated RmPAE (Fig.S1) probably due to the protein unfolding and aggregation. The short-wavelength fluorescence tail around 450 nm in the case of fluorescence excitation in the range from 410 nm to 320 nm may be due to lumichrome emission. The weak fluorescence emission around 400 nm in the case of fluorescence excitation between 330 nm and 310 nm may be due to emission of a quinoxaline hydrolysis product of flavin [24].

The dependence of the fluorescence quantum yield ϕ_F of RmPAE after the heating-cooling cycle on the fluorescence excitation wavelength is shown in Fig.S5. In the range from 480 nm to 350 nm the fluorescence quantum yield is approximately constant at ϕ_F = 0.152±0.003. In the range from 340 nm to 300 nm the fluorescence quantum yield decreases due to additional higher excited state deactivation paths (violation of Kasha-Vavilov rule of excitation wavelength independent fluorescence emission [43,44]). In the range from 290 nm to 270 nm the fluorescence quantum yield is determined by flavin and Trp emission. At shorter excitation wavelength the fluorescence quantum yield is thought to be reduced by higher excited state deactivation paths for Tyr, Trp, and flavin.

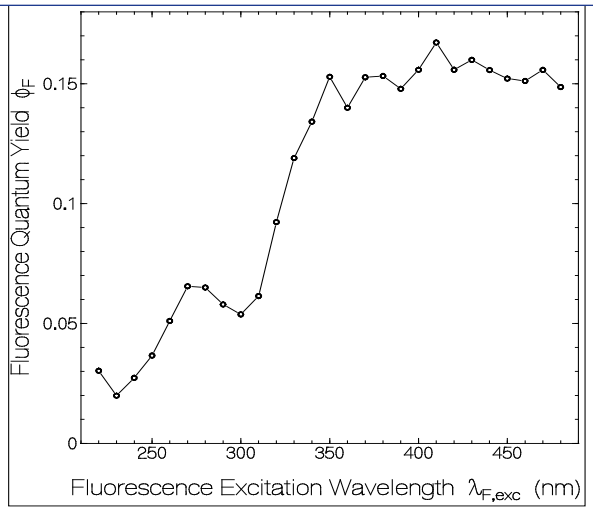

Fig.S5: Dependence of fluorescence quantum yield of RmPAE on fluorescence excitation wavelength after heat denaturing of the sample.

The obtained fluorescence quantum yield of flavin in heat-denatured RmPAE at 450 nm is ϕ_F = 0.152±0.003. Before sample heating the fluorescence quantum yield at 450 nm was ϕ_F = 0.0065±0.0005. The rise in fluorescence quantum yield indicates the release of flavin in the heating process (protein denaturation).

The flavin fluorescence quantum yield $\phi_{F,Fl,denatured}$ = 0.152±0.003 of heat-denatured RmPAE at the flavin fluorescence excitation wavelength of $\lambda_{F,exc}$ = 450 nm is used to estimate the flavin composition in RmPAE. $\phi_{F,Fl,denatured}$ is determined by the mole-fractions x_{FMN} of FMN ($\phi_{F,FMN}$ = 0.23 [16]), x_{RF} of rioflavin ($\phi_{F,riboflavin}$ = 0.26 [27]) and x_{FAD} of FAD ($\phi_{F,FAD}$ = 0.033 [17]). It is

$$\begin{aligned}\phi_{F,Fl,denatured} &= x_{FMN}\phi_{FMN} + x_{RF}\phi_{RF} + x_{FAD}\phi_{FAD} \\ &\approx x_{FMN,RF}\phi_{FMN} + x_{FAD}\phi_{FAD} \\ &= x_{FMN,RF}\phi_{FMN} + (1 - x_{FMN,RF})\phi_{FAD}\end{aligned} \quad \text{(S6)}$$

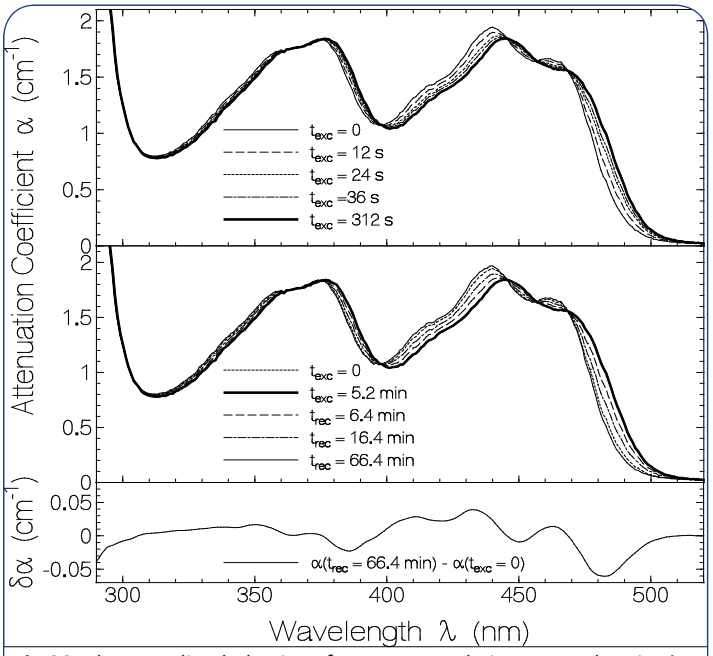

Fig.S6: Photo-cycling behavior of RmPAE sample in a second excitation-recovery cycle (first excitation 25.75 h earlier with I_{exc} = 93.8 mW cm^{-2} for 2.8 min at 455 nm). Temperature ϑ = 23.8 °C. Top part: Attenuation coefficient spectra development during sample exposure at 455 nm with I_{exc} = 0.938 mW cm^{-2}. Exposure times, t_{exc}, of the displayed curves are given in the legend. Middle part: attenuation coefficient spectra development after excitation light switch-off. Bottom part: Attenuation coefficient difference between dark-recovered sample (t_{rec} = 66.4 min) and initial sample (t_{exc} =0).

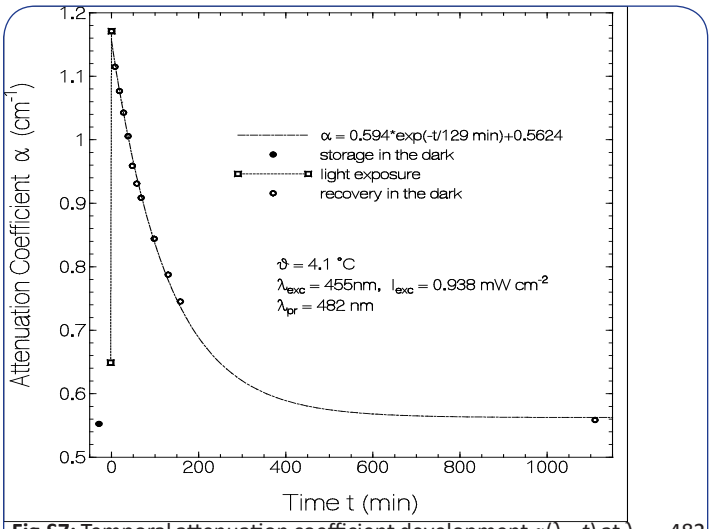

Fig.S7: Temporal attenuation coefficient development α(λ_{pr},t) at λ_{pr} = 482 nm before, during and after RmPAE sample exposure (see main text). Temperature ϑ = 4.1±0.1 °C. Dash-dotted curve is single-exponential fit with τ_{rec} = 129 min.

where $x_{FMN,RF}=x_{FMN}+x_{RF}$ is the mole-fraction of FMN and RF together. From the experimental result of $\phi_{F,\,Fl,\,denatured}$ only mole-fractions $x_{FMN,RF}$ and x_{FAD} = 1- $x_{FMN,RF}$ can be estimated since the fluorescence quantum yields of FMN and riboflavin are nearly the same. Rearrangement of Eq.S6 gives

$$x_{FMN,RF} \approx \frac{\phi_{F,Fl}-\phi_{F,FAD}}{\phi_{F,FMN}-\phi_{F,FAD}} \qquad \text{(S7)}$$

Insertion of values gives $x_{FMN,RF}$ = 0.604±0.015 and x_{FAD} = 0.396±0.015.

S5. BLUF domain signaling state formation and recovery in RmPAE

S5.1. Absorption spectroscopic investigation: The photo-cycling behavior of RmPAE in a second excitation-recovery cycle 25.75 h after the first photo-cycle of Fig.6 is displayed in Fig.S6. The sample was excited at λ_{exc} = 455 nm with I_{exc} = 0.938 mW cm^{-2} for a duration of 5.2 min. The RmPAE signaling state recovery was followed over 66.4 min. The top part of Fig.S6 displays the temporal signaling state formation, the middle part shows the signaling state recovery to the receptor state, and the lower part displays the attenuation coefficient difference between dark recovered sample and initial sample. The absorption spectrum of the dark-adapted sample after t_{rec} = 66.4 min is sharper than the initial absorption spectrum before light exposure. This indicates some irreversible partial protein re-structuring during being in the signaling state.

The temporal attenuation coefficient development at λ_{pr} = 482 nm of RmPAE at ϑ = 4.1±0.1 °C after light exposure at 455 nm with I_{exc} = 0.938 mW cm^{-2} for t_{exc} = 2 min is shown in Fig.S7. At t = -29 min the sample was taken from its dark storage place at 4.1 °C and its absorption and fluorescence spectrum was measured. Then in the time range between t = -2 min and 0 min the sample was exposed at 455 nm with I_{exc} = 0.938 mW cm^{-2}. After that the sample was kept in the dark at 4.1 °C and at the displayed time points sample attenuation spectra were measured. The $\alpha(\lambda_{pr}=482\,nm,t)$ attenuation coefficient recovery from the signaling state to the receptor state fits well to a single exponential curve with time constant τ_{rec}(4.1 °C) = 129 min.

The saturation energy density w_{sat} of light exposure to transfer RmPAE from the receptor state to the signaling state is given by [33]

$$w_{sat} = \frac{h\nu_{exc}}{\sigma_{abs,exc}\phi_s}, \qquad \text{(S8a)}$$

where $\nu_{exc} = c_0/\lambda_{exc}$ is the excitation frequeny. c_0 is the speed of light in vacuum. Insertion of parameters (λ_{exc} = 455 nm, $\sigma_{abs,exc}$ = 4.1×10^{-17} cm^2, ϕ_s = 0.596) gives w_{sat} = 0.0179 J cm^{-2}. The corresponding saturation intensity is

$$I_{sat} = \frac{w_{sat}}{\tau_{rec}} = \frac{h\nu_{exc}}{\sigma_{abs,exc}\tau_{rec}\phi_s}. \qquad \text{(S8b)}$$

Its value at ϑ = 24.7 °C (τ_{rec} = 19.1 min) is I_{sat}(24.7 °C) = 15.6 μW cm^{-2}, and at ϑ = 4.1 °C (τ_{rec} = 129 min) its value is I_{sat}(4.1 °C) = 2.31 μW cm^{-2}.

S5.2. Fluorescence spectroscopic investigations: Three fluorescence quantum distributions belonging to RmPAE of a third photo-cycle run (λ_{exc} = 455 nm, I_{exc} = 0.938 mW cm^{-2}, t_{exc} = 5.8 min, see main text) are depicted in the top part of Fig.S8. The fluorescence was excited at $\lambda_{F,exc}$ = 450 nm. The dotted curve belongs to the situation before light exposure. The solid curve was measured 30 s after excitation light switch-off. It gives the fluorescence situation of the RmPAE BLUF domain in the signaling state. The dashed curve was measured 60 min after excitation light switch-off. It gives the fluorescence situation of the RmPAE BLUF domain in the recovered dark-adapted state.

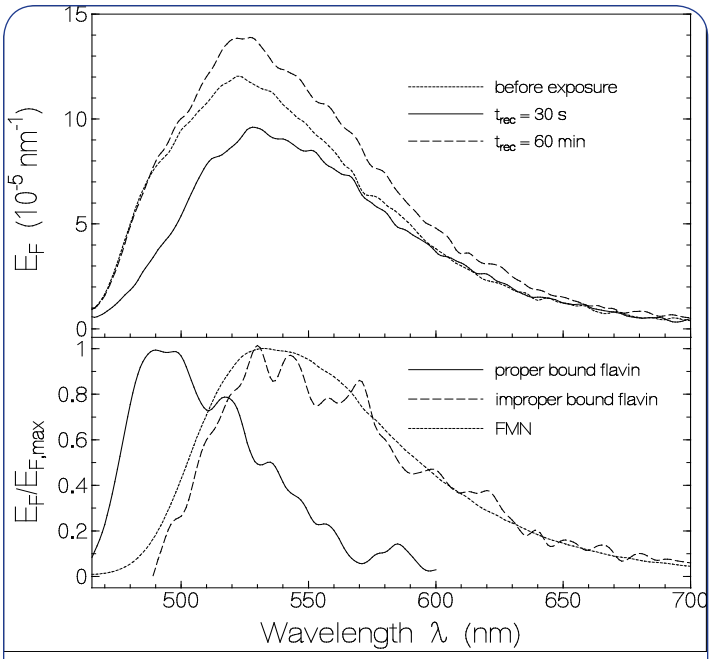

Fig.S8: Top part: Fluorescence quantum distributions of RmPAE belonging to third photo-cycle (see text).

Bottom part: Approximate spectral shapes of fluorescence quantum distributions of proper bound flavin (solid curve), improper bound flavin (dashed curve) and FMN (dotted curve).

The difference between the dotted curve and the solid curve is due to fluorescence emission reduction of proper bound flavin in the signaling state compared to the receptor state. The normalized difference spectrum $\left|E_{F,\,\text{before exposure}}(\lambda)-E_{F,\,t_{rec}=30\,s}(\lambda)\right|/(E_{F,\,\text{before exposure}}-E_{F,\,t_{rec}=30\,s})_{max}$ is shown by the solid curve in the bottom part of Fig.S8. It gives approximately the shape of the fluorescence quantum distribution of flavin in the proper bound state (assuming the same shape of proper bound flavin in the receptor state and the signaling state). The difference between the dashed curve and the dotted curve in the top part of Fig.S8 is due to proper bound flavin release to improper

bound flavin in the BLUF domain signaling state. The dashed curve in the bottom part of Fig.S8 shows the normalized difference spectrum $\left[E_{F,\,t_{rec}=60\,min}(\lambda)-E_{F,\,before\,exposure}(\lambda)\right]/(E_{F,\,t_{rec}=60\,min}-E_{F,\,before\,exposure})_{max}$ It gives the shape of the fluorescence quantum distribution of improper bound flavin. The dotted curve in the bottom part of Fig. S8 shows the shape of the fluorescence quantum distribution of FMN in aqueous solution at pH 7. The fluorescence spectrum of proper bound flavin is approximately 27 nm blue-shifted compared to FMN, while the shape of the fluorescence spectrum of improper bound flavin roughly agrees with the shape of FMN.

The fluorescence quantum yield recovery, shown in the middle part of Fig.8, follows the relation

$$\phi_F(t)=\phi_F(0)+\Delta\phi_F\left[1-\exp\left(-\frac{t}{\tau_{\phi_F,rec}}\right)\right] \qquad \text{(S9a)}$$

with

$$\frac{1}{\tau_{\phi_F,rec}}\approx\frac{1}{\tau_{rec}}+\frac{1}{\tau_{rel}} \qquad \text{(S9b)}$$

where τ_{rel} is the time constant of proper non-covalently bound flavin release in the signaling state to improper bound flavin. Rewriting Eq.S9b gives

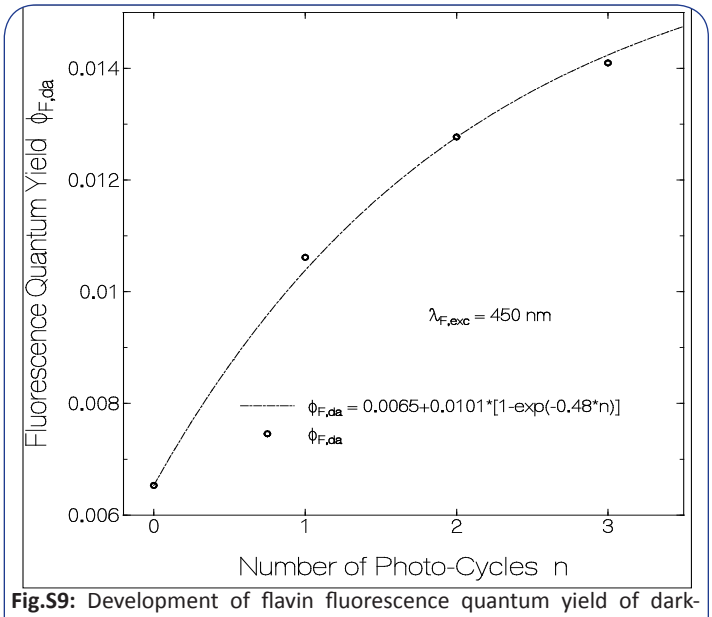

Fig.S9: Development of flavin fluorescence quantum yield of dark-adapted RmPAE on the number of photo-cycles.

$$\tau_{rel}\approx\frac{\tau_{\phi_F,rec}\tau_{rec}}{\tau_{rec}-\tau_{\phi_F,rec}}. \qquad \text{(S9c)}$$

Insertion of the values τ_{rec} = 19.1 min and $\tau_{\phi_F,rec}$ = 12.91 min gives τ_{rel} = 39.8 min (temperature $\vartheta \approx 24.5$ °C).

The dependence of the flavin fluorescence quantum yield in dark-adapted RmPAE on the number of photo-cycles *n* is depicted in Fig.S9. The circles show the development of total dark-adapted fluorescence quantum yield $\phi_{F,da}$. The dash-dotted fit curve is given by

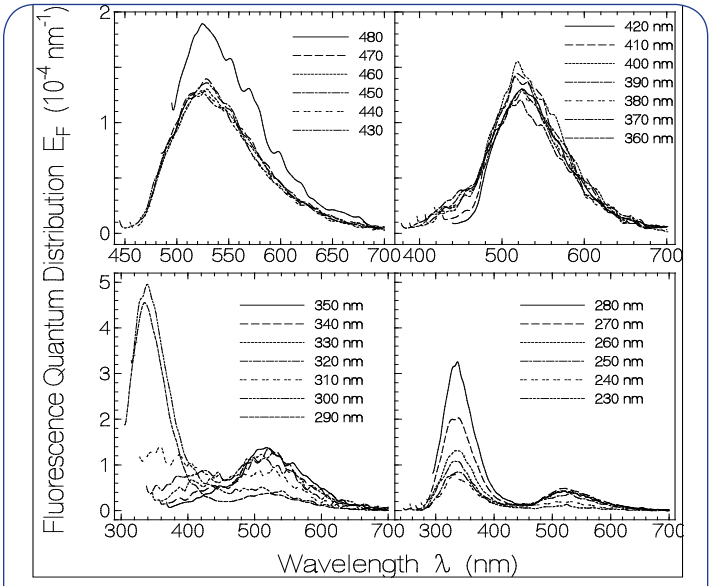

Fig.S10: Fluorescence quantum distributions of RmPAE measured 18 h after third photo-cycle (total accumulated excitation energy density in the three photo-cycles $w_{exc,accum}$ = 16.37 J cm^{-2}). The various fluorescence excitation wavelengths are given in the legends of the subfigures.

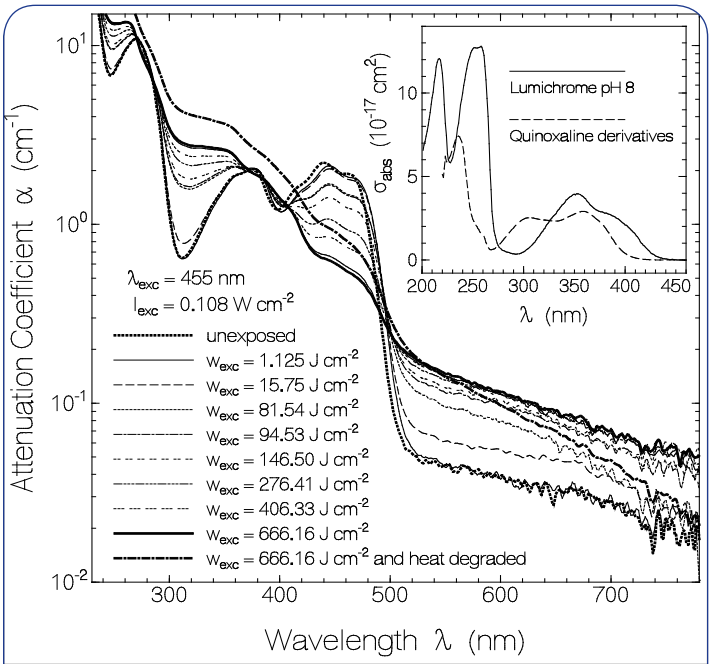

Fig.S11: Attenuation coefficient spectra of RmPAE due to light exposure at 455 nm with I_{exc} = 0.108 W cm^{-2}. Accumulated exposed excitation energy densities w_{exc} are listed in the legend. Temperature ϑ = 23.8±0.5 °C. The inset shows absorption cross-section spectra of lumichrome in aqueous solution at pH 8 (from [22]) and of quinoxaline derivatives (from [23]).

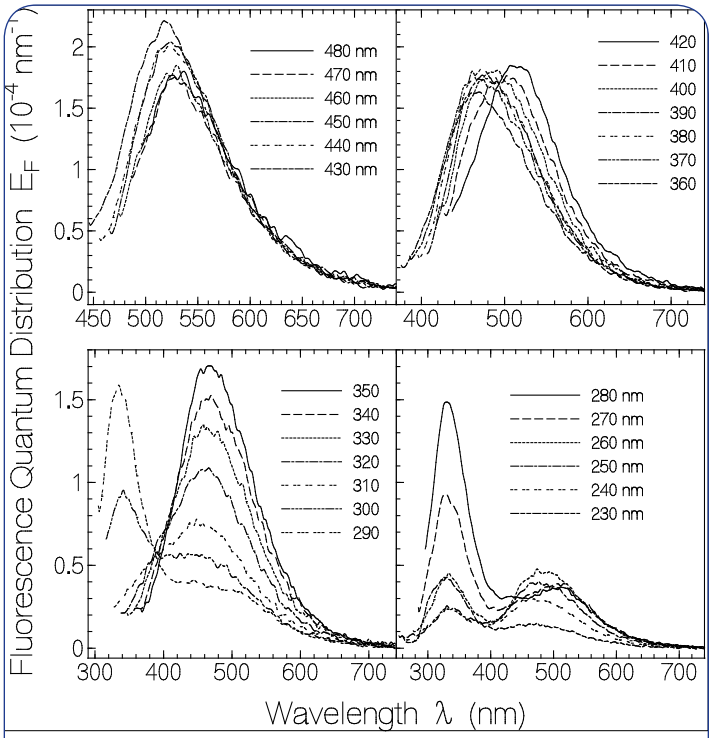

Fig.S12: Fluorescence quantum distributions $E_F(\lambda)$ of RmPAE after photo-degradation. Accumulated exposed energy density w_{exc} = 666.16 J cm^{-2}. The different fluorescence excitation wavelengths $\lambda_{F,exc}$ are given in the legends of the subfigures.

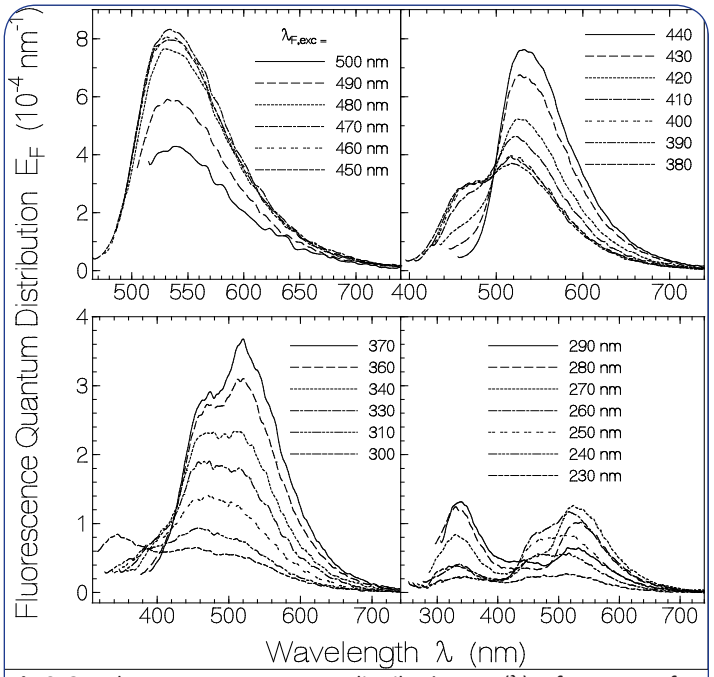

Fig.S13: Fluorescence quantum distributions $E_F(\lambda)$ of RmPAE after photo-degradation ($w_{exc,accum}$ = 666.16 J cm^{-2}) and subsequent heat denaturing. The different fluorescence excitation wavelengths $\lambda_{F,exc}$ are given in the legends of the subfigures.

$$\phi_{F,da}(n) = \phi_{F,da}(0) + \Delta\phi_{F,da,\infty}\left[1 - \exp\left(-\frac{\tau_{rec}}{\tau_{rel}}n\right)\right], \qquad \text{(S10)}$$

with $\Delta\phi_{F,da,\infty}$ = 0.0101 and τ_{rec}/τ_{rel} = 0.48 (τ_{rec} = 19.1 min, τ_{rel} = 39.8 min). $\Delta\phi_{F,da,\infty}$ is related to the fraction $\delta N_{Fl,b,p,\infty}/N_{Fl,0}$ of proper non-covalently bound flavin released in an infinite number of photo-cycles ($n \to \infty$) by

$$\Delta\phi_{F,da,\infty} = \frac{\delta N_{Fl,b,p,\infty}}{N_{Fl,0}} \frac{\tau_{F,b\,ip} - \bar{\tau}_{F,b,p,da}}{\tau_{rad,Fl}}. \qquad \text{(S11a)}$$

Rewriting of Eq.S11a gives

$$\frac{\delta N_{Fl,b,p,\infty}}{N_{Fl,0}} = \Delta\phi_{F,da,\infty} \frac{\tau_{rad,Fl}}{\tau_{F,b\,ip} - \bar{\tau}_{F,b,p,da}}. \qquad \text{S11b)}$$

Insertion of numbers ($\tau_{F,b,ip} \approx$ 500 ps (see Fig.5), $\bar{\tau}_{F,b,p,da} \approx$ 41.5 ps, $\tau_{rad,Fl}$ = 19 ns and $\Delta\phi_{F,b,p,\infty}$ = 0.0101 gives $\delta N_{F,b,p,\infty}/N_{Fl,0} \approx$ 0.419. The fraction of flavin cofactor $\delta N_{F,b,p,\infty}/N_{Fl,0}$ is within experimental accuracy equal to the mole-fraction of FAD in the flavin composition (χ_{FAD} =0.396±0.015).

The excitation wavelength dependence of the dark-adapted fluorescence quantum yield $\phi_{F,da}$ after three photo-cycles is shown by the dotted-line connected triangles in Fig.S2.

Fluorescence quantum distributions of dark-adapted RmPAE after three photo-cycles for different fluorescence excitation wavelengths in the range from 480 nm to 230 nm are displayed in Fig.S10. Compared to the fluorescence quantum distributions of fresh unexposed RmPAE (Fig.S1) the main difference is the increased flavin emission due to the release of proper non-covalently bound flavin in the RmPAE BLUF domain to improper non-covalently bound flavin. The emission around 450 nm is increased likely due to some photo-degradation of flavin to lumichrome. The emission around 400 nm is increased likely due to some photo-degradation of flavin to quinoxaline hydrolysis products.

S6. Photo-degradation of RmPAE in the signaling state

In Fig.S11 the development of the attenuation coefficient spectrum of RmPAE due to light exposure at λ_{exc} = 455 nm with I_{exc} = 0.108 W cm^{-2} is shown. Accumulated exposed excitation energy densities w_{exc} are listed in the legend. The thick dotted curve belongs to the unexposed sample (sample in receptor state). The thin solid curve represents the sample in the signaling state (sample exposed with w_{exc} = 1.15 J cm^{-2}, negligible degradation in signaling state). The thick solid curve shows the attenuation coefficient spectrum at the end of the light exposure (accumulated exposed energy density w_{exc} = 666.16 J cm^{-2}). The thick dash-dotted curve shows the attenuation coefficient spectrum of the sample which was heat denatured three days after the photo-degradation (sample inserted in heat bath at 66.3 °C and heated up to 85.6 °C within 10 min, then cooled down and centrifuged at 4 °C for 15 min with 4400 rpm).

The inset in Fig.S11 shows the absorption cross-section spectra of lumichrome in aqueous solution at pH 8 (from [22]) and of quinoxaline derivatives (from [23]).

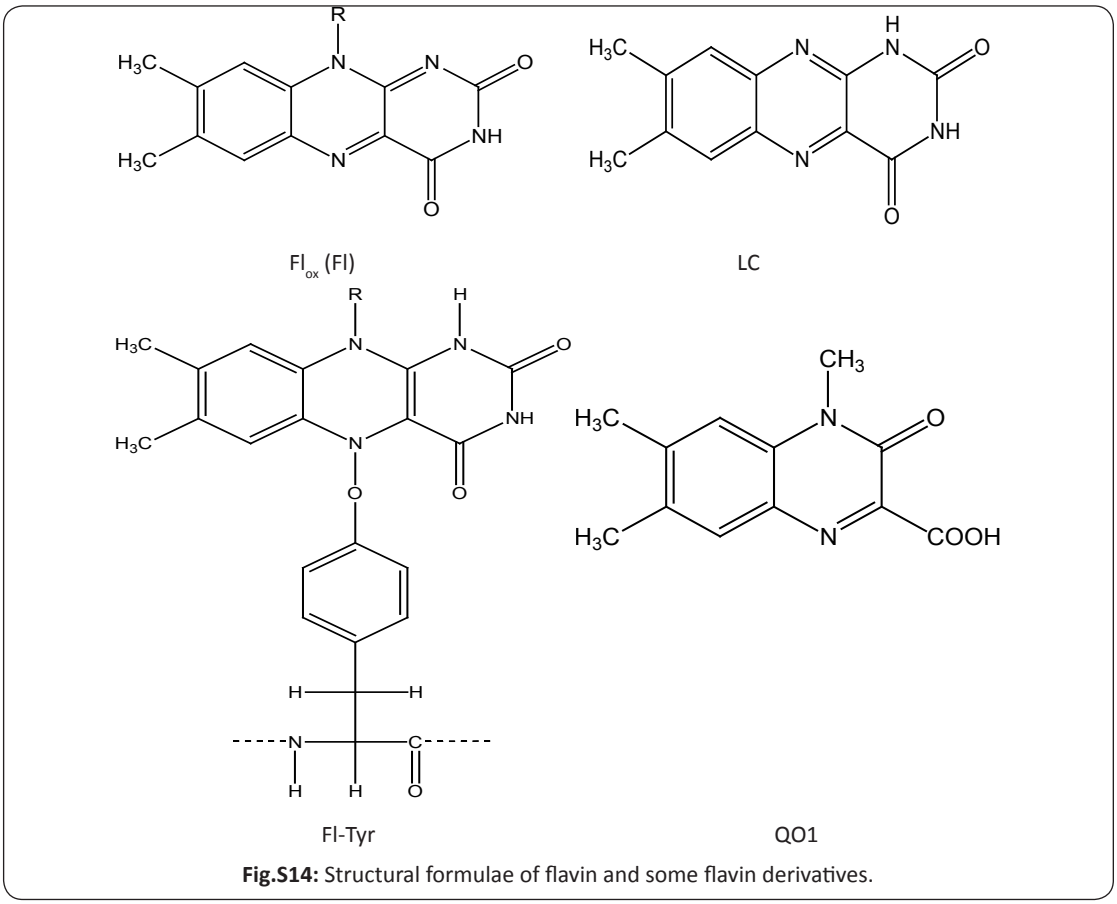

Fig.S14: Structural formulae of flavin and some flavin derivatives.

In Fig.S12 fluorescence quantum distributions $E_F(\lambda)$ of RmPAE after photo-degradation (see Fig.S11) are shown in the range from λ_{Fexc} = 480 nm to 230 nm in steps of 10 nm. In Fig.S13 the fluorescence quantum distributions are shown after additional heat denaturing of RmPAE.

S7. Structural formulae of some involved flavins: Structural formulae of fully oxidized flavin Fl$_{ox}$ (flavin quinone Fl), lumichrome LC, (reduced) flavin – tyrosinyl adduct Fl-Tyr, and a quinoxaline derivative QO1 (1,2-dihydro-2-keto-1,6,7-trimethyl-quinoxaline-3-carboxylic acid) are shown in Fig.S14.

Summary

The pink to light reddish-pigmented bacterium *Rubellimicrobium mesophilum* strain MSL-20^T contains a BLUF coupled endonuclease III (BLUF-EndoIII) of unknown function. This BLUF-EndoIII protein was identified through metagenome analysis by Conserved Domain Search in NCBI portal. A sequence alignment study of the BLUF domain of BLUF-EndoIII with the BLUF domain of AppA from *Rhodobacter sphaeroides* indicated that three essential flavin binding amino acids for BLUF activity were different. Therefore a purified recombinant triple mutated BLUF coupled endonuclease III (F5Y, N27H, A87W) named RmPAE (*Rubellimicrobium mesophilum* Photo-Activated Endonuclease) was expressed in *Escherichia coli*, and it was characterized by absorption and emission spectroscopic methods.

The flavin cofactor loading was determined by absorption spectrum analysis to be about 26 %. The flavin composition was deduced from fluorescence quantum yield measurement of heat denatured RmPAE to be approximately 60 % of FMN (and/or riboflavin) and 40 % FAD.

The primary BLUF domain photo-cycling behavior of RmPAE starting from its receptor state was similar to other BLUF proteins studied thus far. The first flavin absorption band spectral red-shift in the signaling state of about 5.4 nm was rather small, and the signaling state recovery to the receptor state after light switch-off of about 19 min at room temperature was rather long. Different to other BLUF proteins, for RmPAE in the signaling state, there occurred partial removal of BLUF active flavin in proper non-covalently bound position to BLUF inactive flavin in improper position (likely FAD cofactor re-localization).

The receptor-state signaling-state photo-cycling dynamics is presented in a refined photo-cycle scheme and a ground-state and excited-state reaction coordinate scheme. Energetic and kinetic parameters are extracted.

Photo-excitation of RmPAE in its light-adapted signaling state (secondary BLUF domain photo-cycling) caused low-efficient permanent covalent reduced flavin – Tyr adduct formation and conversion of flavin to lumichrome and quinoxaline derivatives.

References

1. Dastager SG, Lee JC, Ju YJ, Park DJ, Kim CJ (2008) *Rubellimicrobium mesophilum* sp. nov., a mesophilic, pigmented bacterium isolated from soil. Syst Evol Microbiol 58: 1797-1800.

2. Wagner-Döbler I, Biebl H (2006) Environmental biology of the marine *Roseobacter* lineage. Annu Rev Microbiol 60: 255-280.

3. Riedel T, Spring S, Fiebig A, Petersen J, Göker M, et al. (2014) Genome sequence of the pink to light reddish–pigmented *Rubellimicrobium mesophilum* type strain (DSM 19309^{T}), a representative of the *Roseobacter* group isolated from soil, and emended description of the species. Standards in Genomic Sciences 9: 902-913.

4. Marchler-Bauer A, Anderson JB, Chitsaz F, Derbyshire MK, DeWeese-Scott C, et al. (2009) CDD: specific functional annotation with the conserved domain database. Nucleic Acids Res 37: D205-D210.

5. Anderson S, Dragnea V, Masuda S, Ybe J, Moffat K, Bauer C (2005) Structure of a novel photoreceptor, the BLUF domain of AppA from *Rhodobacter sphaeroides*. Biochem 44: 7998-8005.

6. Hall TA (1999) BioEdit: a user-friendly biological sequence alignment editor and analysis program for Windows 95/98/NT. Nucleic Acids Symposium Series 41: 95-98.

7. Zoltowski BD, Gardner KH (2011) Tripping the light fantastic: blue-light photoreceptors as examples of environmentally modulated protein-protein interactions. Biochem 50: 4-16.

8. Losi A, Gärtner W (2011) Old chromophores, new photoactivation paradigms, trendy applications: flavins in blue light-sensing photoreceptors. Photochem Photobiol 87: 491-510.

9. Masuda S (2013) Light detection and signal transduction in the BLUF photoreceptors. Plant Cell Physiol 54: 171-179.

10. Penzkofer A, Tanwar M, Veetil SK, Kateriya S (2014) Photo-dynamics of photoactivated adenylyl cyclyse LiPAC from the spirochete bacterium *Leptonema illini* strain 3055^{T}. Trends in Applied Spectroscopy 11: 39-62.

11. Förster T (1951) Fluoreszenz organischer Verbindungen. Vandenhoeck und Ruprecht, Germany, Göttingen.

12. Penzkofer A (2012) Photoluminescence behavior of riboflavin and lumiflavin in liquid solutions and solid films. Chem Phys 400: 142-153.

13. Sens R (1984) Strahlungslose Desaktivierung in Xanthen, Oxazin und Carbazinfarbstoffen. Dissertation Universität-Gesamthochschule Siegen, Germany.

14. Penzkofer A, Stierl M, Hegemann P, Kateriya S (2011) Thermal protein unfolding in photo-activated adenylate cyclase nano-clusters from the amoeboflagellate *Naegleria gruberi* NEG-M strain. J Photochem Photobiol A: Chem 225: 42-51.

15. Penzkofer A, Shirdel J, Zirak P, Breitkreuz H, Wolf E (2007) Protein aggregation studied by forward light scattering and light transmission analysis. Chem Phys 342: 55-63.

16. Holzer W, Shirdel J, Zirak P, Penzkofer A, Hegemann P, et al. (2005) Photo-induced degradation of some flavins in aqueous solution. Chem Phys 308: 69-78.

17. Islam SDM, Susdorf T, Penzkofer A, Hegemann P (2003) Fluorescence quenching of flavin adenine dinucleotide in aqueous solution by pH dependent isomerisation and photo-induced electron transfer. Chem Phys 295: 137-149.

18. Lindsey J, PhotochemCAD Spectra by Category.

19. Müller F (Ed.) (1991) Chemistry and biochemistry of flavoenzymes. Vol. 1, CRC Press, USA, Boca Raton.

20. Penzkofer A, Stierl M, Hegemann P, Kateriya S (2012) Absorption and fluorescence characteristics of photo-activated adenylate cyclase nano-clusters from the amoeboflagellate *Nagleria gruberi* NEG-M strain. Chem Phys 392: 46-54.

21. Penzkofer A, Tanwar M, Veetil SK, Kateriya S, Stierl M, et al. (2013) Photodynamics and thermal behavior of the BLUF domain containing adenylate cyclase NgPAC2 from the amoeboflagellate *Nagleria gruberi* NEG-M strain. Chem Phys 412: 96-108.

22. Tyagi A, Penzkofer A (2011) Absorption and emission spectroscopic characterization of lumichrome in aqueous solutions. Photochem Photobiol 87: 524-533.

23. Penzkofer A, Tyagi A, Kiermaier J (2011) Room temperature hydrolysis of lumiflavin in alkaline aqueous solution. J Photochem Photobiol A: Chem 217: 369-375.

24. Penzkofer A, Luck M, Mathes T, Hegemann P (2014) Bistable retinal Schiff base photo-dynamics of histidine kinase rhodopsin HKR1 from *Chlamydomonas reinhardtii*. Photochem Photobiol 90: 773-785.

25. Chen RF (1967) Fluorescence quantum yields of tryptophan and tyrosine. Analytical Letters 1: 35-42.

26. Zirak P, Penzkofer A, Hegemann P, Mathes T (2007) Photo dynamics of BLUF domain mutant H44R of AppA from *Rhodobacter sphaeroides*. Chem Phys 335: 15-27.

27. Drössler P, Holzer W, Penzkofer A, Hegemann P (2002) pH dependence of the absorption and emission behaviour of riboflavin in aqueous solution. Chem Phys 282: 429-439.

28. Fleming GR (1986) Chemical applications of ultrafast spectroscopy. Oxford University Press, USA, New York.

29. Voet D, Voet JG (2004) Biochemistry. 3rd ed., Wiley & Sons, USA, Chapter 14.

30. Heuts DPHM, Scrutton NS, McIntire WS, Fraaije MW (2009) What's in a covalent bond? On the role and formation of covalently bound flavin cofactors. FEBS J 276: 3405-3427.

31. Penzkofer A, Tanwar M, Veetil SK, Kateriya S (2015) Photo-dynamics of photoactivated adenylyl cyclase TpPAC from the spirochete bacterium *Turneriella parva* strain H^{T}. J Photochem Photobiol B: Biol 153: 90-102.

32. Song SH, Dick B, Penzkofer A (2007) Photo-induced reduction of flavin mononucleotide in aqueous solutions. Chem Phys 332: 55-65.

33. Penzkofer A, Stierl M, Mathes T, Hegemann P (2014) Absorption and emission spectroscopic characterization of photo-dynamics of photoactivated adenylyl cyclase mutant bPAC-Y7F of *Beggiatoa* sp.. J Photochem Photobiol B: Biol 140: 182-193.

34. Miura R (2001) Versatility and specifity in flavoenzymes: control mechanisms of flavin reactivity. The Chemical Record 1: 183-194.

35. Lin TY, Werther T, Jeoung JH, Dobbek H (2012) Suppression of electron transfer to dioxygen by charge transfer and electron transfer complexes in the FAD-dependent reductase component of toluene dioxygenase. J Biol Chem 287: 38338-38346.

36. Van den Berg PAW, Feenstra KA, Mark AE, Berendsen HJC, Visser AJWG (2002) Dynamic conformations of flavin adenine dinucleotide: simulated molecular dynamics of the flavin cofactor related to the time-resolved fluorescence characteristics. J Phys Chem B 106: 8858-8869.

37. Nakabayashi T, Islam MS, Ohta N (2010) Fluorescence decay dynamics of flavin adenine dinucleotide in a mixture of alcohol and water in the femtosecond and nanosecond time range. J Phys Chem B 114: 15254-15260.

38. Penzkofer A, Stierl M, Hegemann P, Kateriya S (2011) Photo-dynamics of the BLUF domain containing soluble adenylate cyclase (nPAC) from the amoeboflagellate *Naegleria gruberi* NEG-M strain. Chem Phys 387: 25-38.

39. Penzkofer A, Shirdel J, Zirak P, Breitkreuz H, Wolf E (2007) Protein Aggregation studied by forward light scattering and light transmission analysis. Chem Phys 342: 55-63.

40. Fischer H, Polikarpov I, Craievich A (2004) Average protein density is a molecular-weight-dependent function. Protein Sci 13: 2825-2828.

41. Barer R, Tkaczyk S (1954) Refractive index of concentrated protein solutions. Nature 173: 821-822.

42. Laan W, Bednarz T, Heberle J, Hellingwerf KJ (2004) Chromophore composition of a heterologously expressed BLUF-domain. Photochem Photobiol Sci 3: 1011-1016.

43. Vavilov SI (1927) Die Fluoreszenzausbeute von Farbstofflösungen als Funktion der Wellenlänge des anregenden Lichtes. Z Phys 42: 311-318.

44. Lewis GN, Kasha M (1944) Phosphorescence and the triplet state. J Am Chem Soc 66: 2100-2116.